J Sol-Gel Sci Technol (2016) 77:1–27
DOI 10.1007/s10971-015-3879-x

REVIEW PAPER

Cleaning and anti-reflective (AR) hydrophobic coating of glass surface: a review from materials science perspective

Tania Dey[1] · **Daragh Naughton**[1]

Received: 29 May 2015 / Accepted: 29 September 2015 / Published online: 30 October 2015

Abstract This article reviews the principles, mechanisms and comparisons of glass surface cleaning by various wet chemical and dry cleaning methods, including acid–base–solvent combinations, HF etching, chelation, vapor degreasing, UV–ozone, oxygen plasma, heating/pyrolysis, ultrasonic and laser treatments. This article also covers four major hydrophobic coating strategies, namely hydrosilylation, silanization, plasma treatment and DC sputtering, along with their process-wise applications. A special emphasis is given on the silanization process: its mechanism, factors affecting, choices of solvents and precursors, and limitations, which is utilized in anti-reflective (AR) sol–gel coating formation as well. Some of the common surface analytical techniques, its utility and reported data has also been reviewed in this context. Finally, a section has been devoted to anti-reflective (AR) and transmittance properties, elucidating the theory and methods of AR coating generation, factors affecting and related literature reports. The challenge lies in coming up with non-harsh cleaning procedures and water-based hydrophobic coatings, with an eye for application in ecological proximity.

Graphical Abstract

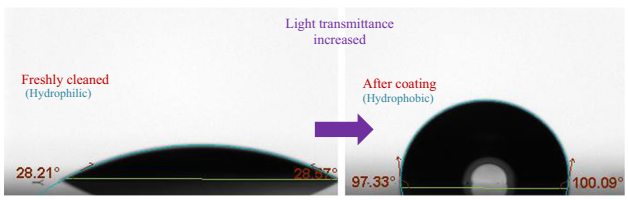

✉ Tania Dey
taniadey@hotmail.com

[1] Department of Mechanical Engineering, Limerick Institute of Technology, Moylish Park, Limerick, Ireland

Keywords Surface cleaning · Glass · Hydrophobic · Anti-reflective · Silanization · Sol–gel coating

1 Introduction

In the world of materials, most of the interesting phenomena occur on the surfaces. Hence, surface modification becomes of great importance to scientists working in the multi-disciplinary areas. Glass surfaces are mostly made of silica (SiO_2) and find use in greenhouses, windows, windshields, monitors, reading glasses, drinking glasses, camera lenses and mirrors. Common materials that contaminate glass surfaces are dust, dirt, metals and oils, giving rise to a weathered look.

A glass surface can be of three types: (a) flat, e.g., single-crystal silicon wafer used in microelectronics, (b) curved, e.g., amorphous nanoparticles used in photovoltaics and (c) porous, e.g., aerogels used for low dielectric applications and CO_2 capture technologies. The forces that are involved in glass modification can either be chemical or physical in nature or a combination of both. Besides, surface interactions with water must compete with a variety of internal interactions of liquid phase water: van der Waals forces, dipole interactions, hydrogen bonding and proton exchange.

Functionalization is the process of adding new functions, features, capabilities or properties to a material by changing the surface chemistry of the material. Glass functionalization is ideal for converting the hydrophilic surface into a hydrophobic one, changing its zeta potential, changing color, rendering the surface antifungal and even decorating the glass surface with specific patterns.

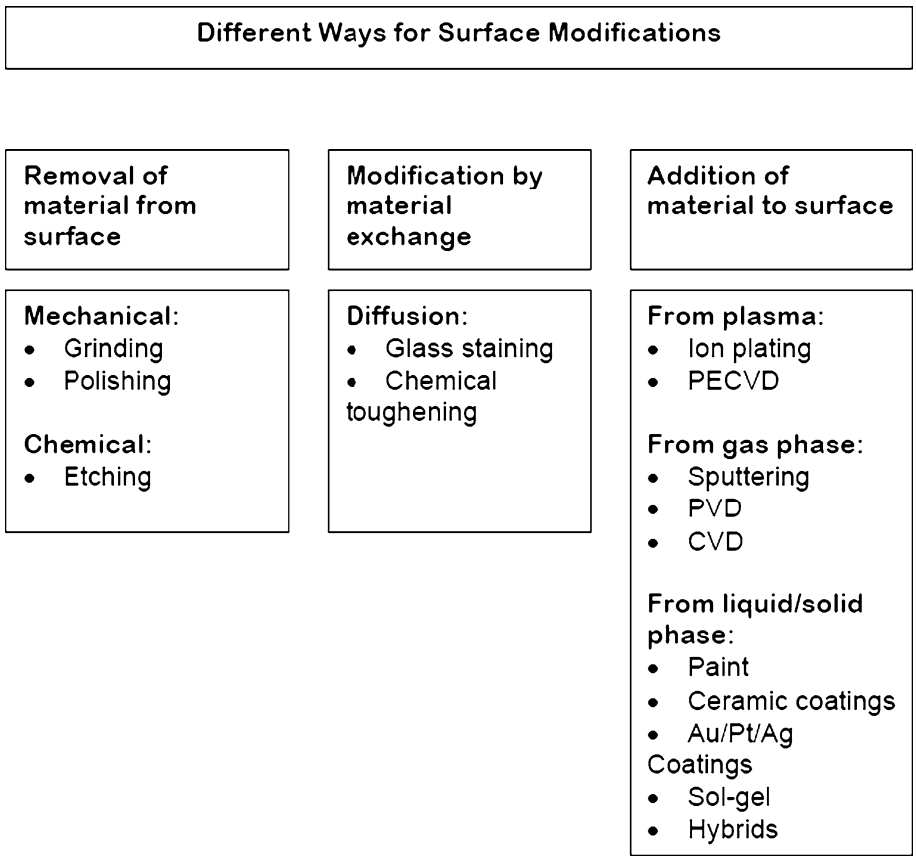

Fig. 1 Ways of glass surface modification. Reprinted with permission from [1]. Copyright: Ferdinand Trier

The condition of the glass surface depends to a great extent on the history of the glass. It changes not only during manufacturing, but also during storage. A nice summary of different methods of glass surface modification is shown in Fig. 1 [1].

The purpose of this review is to compare the existing methods of glass surface cleaning and hydrophobic modification in water medium, using contact angle and various other techniques as a tool for assessment and come up with the most optimized method suitable for application in eco-friendly areas. In this context, development of anti-reflective (AR) sol–gel coatings on glass surface will also be discussed.

As far as surface coating strategies are concerned, they will be organized and discussed here in a slightly different manner than Fig. 1. Also to cut it short, surface patterning and curved surfaces will be deliberately excluded from our discussion.

2 Cleaning methods

Surface cleanliness is of key importance to surface scientists. To achieve optimal uniformity and reproducibility, the surface must be free from any contaminants and the reactive hydroxyls of glass (silica) must be activated [2, 3]. It is also recommended to immediately coat the surface after cleaning. The cleaning methods found in literature [4–7] utilize various combinations of acids, bases and organic solvents at different times, strengths and temperatures, which can be categorized as wet chemical methods. Other wet chemical methods include HF etching [8–12], chelation [13, 14] and vapor degreasing [15]. Furthermore, there are dry methods of glass cleaning such as UV–ozone [16–20], oxygen plasma [21–26], pyrolysis [27] and laser treatment [28–30]. Besides mechanical polishing such as chalk scrubbing is sometimes used as a pre-cleaning step. However, there is no universally accepted cleaning agent or method till date.

Cleanliness of a glass surface can be quantified by contact angle measurement (angle made by the tangent to the drop at its intersection with the slide surface), usually 10–20 s after the formation of water sessile drop. An effective cleaning method should produce a very hydrophilic surface with low water contact angle [31, 32]. Literature values show a wide variation in contact angles ($\sim$7° to 92°) as many groups have reported advancing and receding contact angles instead of equilibrium contact angles. This method remains a relatively quick and easy method for assessing glass surface cleanliness,

Table 1 Different wet chemical methods of glass cleaning used by Cras et al. Reprinted with permission from [4]. Copyright: 1999 Elsevier

Method	Steps
1	30 min in 1:1 MeOH:HCl
	Rinse in H_2O, dry under N_2
2	Method 1 + additional incubation (30 min) in conc. H_2SO_4
	Rinse in H_2O, dry under N_2
3	Method 2 + additional incubation (30 min) in 100 °C H_2O
	Dry under N_2
4	5 min in 1:1:5 NH_4OH:H_2O_2 (30 %):H_2O at 80 °C
	Rinse in H_2O, dry under N_2
5	Method 4 + additional incubation (5 min) in 1:1:5 HCl:H_2O_2 (30 %):H_2O at 80 °C
	Rinse in H_2O, dry under N_2
6	30 min in 10 % KOH in isopropanol
	Rinse in H_2O, dry under N_2
7	20 min in 1 M NaOH
	Rinse in H_2O, dry under N_2
8	Method 7 + additional incubation (30 min) in piranha (1:2 H_2O_2:H_2SO_4)
	Rinse in H_2O, dry under N_2

whereas the efficiency of cleaning methods can be further verified by XPS, AFM, ellipsometry and FTIR [5].

2.1 Wet chemical methods

2.1.1 Combination of acids, bases and solvents

For initial cleaning, it is customary to rinse the surfaces with ethanol and sonicate for 5 min in 2 % Hellmanex (15–30 % tripotassium orthophosphate solution), and then rinse with Milli-pore water (18.2 MV, Millipore Inc.) and finally sonicate for 3 min in Milli-pore water. After these steps, the glass samples can be immersed for 30 min in the different activation solutions as mentioned in Table 1 [4] and finally dried under inert gas (argon or nitrogen). Results of this study are shown in Fig. 2.

Cleaning by use of ammonia and hydrogen peroxide mixture is called remote chemical analysis (RCA) and is widely used in semiconductor industry.

The activation solutions in another study [5] contained the following, the results being shown in Table 2:

A. MeOH/HCl $[V : V = 1 : 1]$ B. Method A + conc. H_2SO_4 C. Piranha $[30\%\ H_2O_2$: conc. $H_2SO_4 = 1 : 3]$ D. Conc. H_2SO_4 E. $K_2Cr_2O_7$ + H_2SO_4 F. 1 M NaOH.

Iglauer et al. [7] offers another set of similar cleaning conditions in their review. Using paper towels for absorbing water, as reported in [33], may compromise cleanliness although it came out as the best procedure in that lot. They have used sulfuric acid containing 10 % Nochromix, the compound Nochromix from Godax Lab being proprietary and hence undisclosed by the manufacturer. The MSDS datasheet identifies it as a peroxygen compound, leading us to believe that the activator mixture is similar to Piranha (H_2O_2:H_2SO_4). However, piranha solution is a serious health and safety hazard and not ideal for using in close contact with vegetation such as in greenhouses.

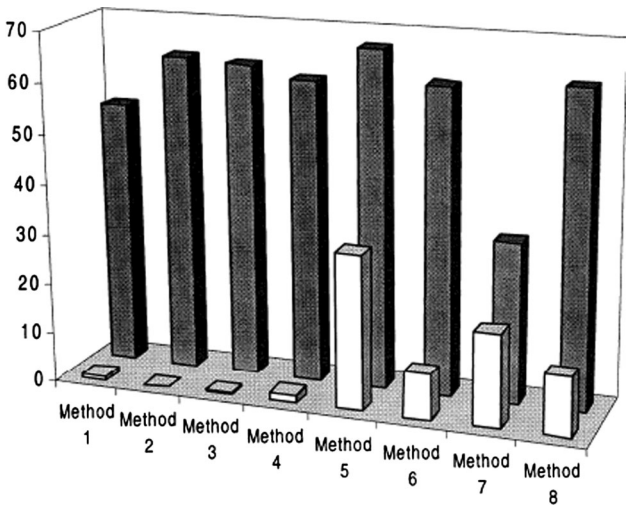

Fig. 2 Mean contact angles of glass slides after cleaning (*white bars*) and after silane treatment (*gray bars*). Reprinted with permission from [4]. Copyright: 1999 Elsevier

Table 2 Contact angles, roughness measured by AFM and etching rates measured by ellipsometry for different wet chemical cleaning methods. Reprinted with permission from [5]. Copyright: 2006 Elsevier

Contact angles, roughness values measured by AFM and etching rates measured by IE for the different wet activation produces						
	CA ($n = 20$)	R_q (nm)	SAD (%)	Thickness loss (nm)	Harmful to encapsulation	CA ($n = 20$) APTES
Original SiO_2 surface	47.7°	0.12	0.01	–	–	–
A MeOH/HCl	24.6°	0.11	0.01	0.4	No	37.1°
B A + conc. H_2SO_4	16.9°	1.66	0.18	0.8	Yes	38.9°
C piranha	24.2°	0.11	0.01	0.6	Yes	54.9°
D Conc. H_2SO_4	16.9°	0.29	0.08	0.8	Yes	64.6°
E $K_2Cr_2O_{7+}H_2SO_4$	11.7°	0.24	0.06	0.7	Yes	54.2°
F 1 M NaOH	37.6°	0.16	0.02	0.9	No	66.3°

No matter what wet chemical method is followed, care should always be taken in having an utmost clean surface, keeping in mind that even organic molecules present in the air, on the fingers of the researcher or in the test cell may cause serious surface contamination. Working in glove box under inert atmosphere, handling substrates with forceps all the time and possibly working in a clean room is desirable.

2.1.2 HF etching

As long as oxide is present on the surface, the surface is hydrophilic and the water contact angle is low. The contact angle increases significantly, upon oxide removal and hydrogen termination of the surface. This so-called dewetting is a visible phenomenon and is a good indication of surface cleanliness.

Kondoh et al. [8] performed a 2 % HF dip to their glass samples and observed a sharp lowering of contact angle at pH = 11 probably due to increase in solubility of silica. The saturation contact angle depends on the process conditions such as oxide thickness, implanted species and acceleration voltage. They identified three different phases in the process: regime I, oxide etching at a constant etch rate; regime II, oxide etching with nonlinear time dependence; regime III, surface hydrophobing.

The HF cleaning method may have some limitations. The main problem is that while the rinsing liquid is dried, capillary forces bend the flexible polysilicon microstructures toward the substrate, bringing them into contact and causing stiction of the microstructures when the restoring force cannot counterbalance the attractive force [9, 10].

There are mainly two methods by which this problem can be solved: (a) use of supercritical drying technique using CO_2 (b) using vacuum sublimation drying of a frozen solvent instead of the liquid-to-vapor transition [9]. Other methods of alleviating the problem include the use of low-surface-tension liquids, temporary support, sublimation of the final liquid and the use of anhydrous HF (hydrogen fluoride) gas-phase etching (GPE) technology to remove sacrificial TEOS (tetraethylorthosilicate) oxide [11].

Mechanism In order to understand glass cleaning by HF dip, one needs to understand the HF-silica chemistry behind it. The rate laws can suggest that the rate-determining step for silica dissolution in fluoride solution involves a coordinated attack of a Lewis acid, on the bridging O atom and a Lewis base on the Si atom. This allows a redistribution of electrons from the Si–O bond to form a O–H group and a Si–FH group. Electrochemical study also shows [12] that in ethanol–water (93:7) mixture, the formation of HF and HF_2^- predominates in dilute HF solutions, whereas HF and polyhomoconjugated species, $(HF)_n$ F^-, predominate in the concentrated HF solutions.

2.1.3 Chelation

The most commonly used cleaning method in microelectronics industry is RCA cleaning which consists of two steps: SC1, i.e., treating with a mixture of ammonia, hydrogen peroxide and water, which is very effective in removing particles and organic matter, but causes metal deposition on wafer namely Al^{3+}, Fe^{3+} and Zn^{2+} followed by SC2, i.e., treating with a mixture of hydrochloric acid, hydrogen peroxide and water to get rid of metal contamination [13].

Optimization of the conventional RCA clean by more economic alternatives is essential and that is where chelation comes into play, as a replacement to SC2 step. Moreover, decomposition of hydrogen peroxide in SC1 solutions gives rise to surface roughness and formation of light point defects (LPDs) due to oxygen bubbles sticking to the surface preventing silicon etching [13].

Chelating agents are multidentate ligands that can form coordination complexes by making several bonds with one single metal ion. Examples include EDTA (ethylenediamine

tetraacetic acid), ethylenediamine (en), tartrate, citrate, porphyrin rings of hemoglobin and chlorophyll, and so on. The strength of the bond between a metal ion and a single functional group in a multidentate ligand is about the same order of magnitude as between the bond of the metal ion and the free ligand. The much higher formation constant of multidentate chelates is mainly attributed to the entropic effect ('chelate effect'). The chelate effect increases with the number of complex forming groups available in a molecule.

The basic requirements for a chelating agent to be used in silicon wafers are (a) high stability constant of the metal complex and (b) chemical stability of both the free chelating agent and its metal chelates in highly oxidizing SC1 condition (Fig. 3).

Martin et al. [13] have come up with a new class of chelating agents that are heterocycles containing nitrogen with methylene phosphonic acid groups (cTRAMP) or acetic acid and have compared their cleaning performance with the open-chain analogues with methylene phosphonic acids (Dequest 2060sE) (Fig. 4) and carboxylic acids (Titriplex VE, EDTA). They observed no deposition of chelating agent, no adherence of particles and increase in surface roughness, and less decomposition of H_2O_2 elongating bath lifetime.

Another report on archaeological glass samples [14] shows that EDTA is generally accepted as the most effective chelating agents recommended for cleaning encrustations on durable glass. It was more effective and safe at neutral pH with low concentrations around 5–7 %. The calcareous crusts can safely be removed by using a piranha solution. Citric and tartaric acids appeared of moderate efficiency for cleaning weathered and stable glass. Calgon (Sodium hexametaphosphate) has a tendency to damage corroded and iridescent surfaces and should be avoided when cleaning weathered glass.

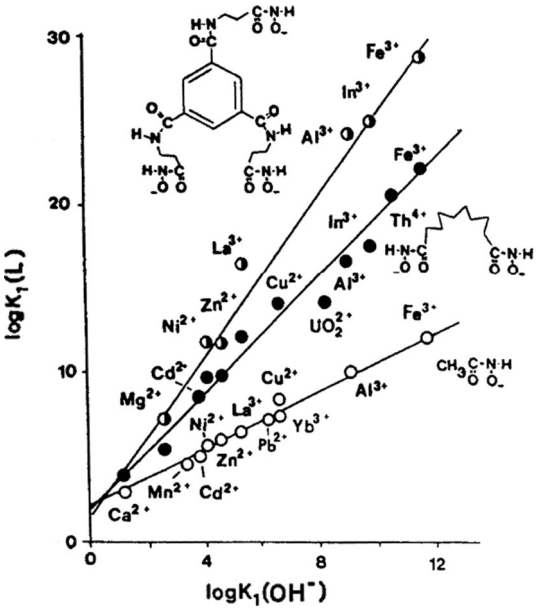

Fig. 3 Relationship between the formation constants of ligands containing negatively charged oxygen donor hydroxamate groups and log K_1 (OH^-) for the metal ions. Reprinted with permission from [13]. Copyright: 1999 Elsevier

2.1.4 *Vapor degreasing*

Vapor degreasing is a process of removing grease and oil films from surfaces. A vapor greasing apparatus consists of an open tank with heating element at the bottom and water condensing coils around the top perimeter [15]. The cleaning solvent can be isopropyl alcohol or some chlorinated/fluorinated hydrocarbon. At high temperature, the solvent forms vapor which remains within the tank due to condensing action. Glass samples are immersed in the vapor for 15 s or more. The solvent vapor has high solvency for fatty contaminants, which drips off by getting replaced with more pure condensing solvent.

2.2 Dry cleaning methods

2.2.1 *UV–ozone*

The capability of ultraviolet (UV) light to decompose organic molecules has been known for a long period of time. In 1972, Bolon and Kuntz [16] reported that UV light can depolymerize a variety of photoresist polymers. During 1974–1976, Vig et al. [17–19] described a series of experiments to find out the variables associated with UV–ozone cleaning such as wavelength of UV radiation,

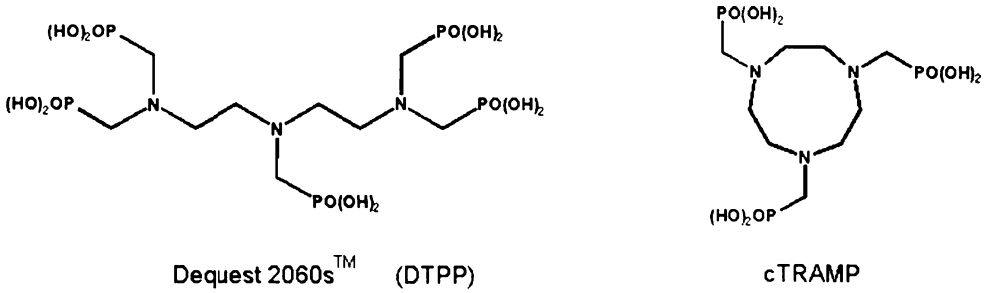

Fig. 4 Chemical structures of some cheating agents used by Martin et al. Reprinted with permission from [13]. Copyright: 1999 Elsevier

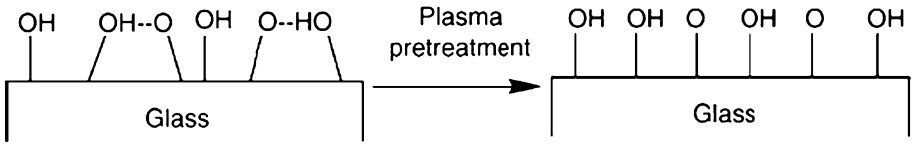

Fig. 5 The change of molecular structure on glass surface after plasma treatment. Reprinted with permission from [21]. Copyright: 2006 Elsevier

distance between sample and UV source, contaminants, pre-cleaning and substrate type.

Mechanism UV–ozone cleaning is primarily a result of photosensitized oxidation process. Atomic oxygen and ozone are produced simultaneously when O_2 is dissociated by absorption of UV of wavelength less than 245.4 nm. Atomic oxygen is also produced when ozone is dissociated by longer wavelength UV radiation. The excited contaminant molecules and free radicals produced by dissociation of contaminant molecules react with atomic oxygen to form simple volatile molecules like CO_2, H_2O and N_2 [20].

Rinsing the glass surface with chloroform, 2-propanol, ethanol, followed by UV–ozone treatment for 30 min is probably the most acceptable method while working in close proximity with food system, as it involves no hazardous compounds at all.

2.2.2 *Oxygen plasma*

Iglauer et al. [7] subjected the glass substrate to 15-min cleaning in air plasma at room temperature ($\sim$296 K). They observed a significant increase in θ due to contamination, if the CO_2 in the cell was decompressed, the cell vacuumed until the water on the quartz crystal fully evaporated and the CO_2 pressure again raised to the experimental value. This was probably caused by residual contamination.

Atmospheric pressure plasma processes are attractive for industrial applications because of their lower cost, higher throughput and ability to operate without vacuum systems [21]. Therefore, they were widely used in pollution control, sterilization, ozone generation and surface modification [22–24]. Authors claim that there is no report of glass surface modification using dielectric barrier discharge (DBD) and middle frequency power supply (16 kHz).

Mechanism The chemical reaction of plasma hydrophilic pre-treatment can be explained according to the molecular structure proposed by Sakuhana [25]. The electron energy of the nonthermal plasma is in the range of 4–5 eV and big enough to break the hydrogen bonds (0.2–0.3 eV) [26]. When plasma is applied, the O–OH bond with shorter distance is divided up by electron impact and atomic oxygen O, and more OH radicals appear on the glass surface as shown in Fig. 3 [21]. These OH radicals are hydrophilic groups, which cause increase in surface energy and decrease in water contact angle, giving rise to super-clean surface (Fig. 5).

2.2.3 *Heating and pyrolysis*

Pyrolysis involves heating up the glass to 300–500 °C for more than 30 min. The heating and subsequent cooling is usually performed in slow ramp in order to avoid glass breakage from thermal shock. This process relies on degradation and desorption of organic contaminants like fluorocarbons, but is not good for removing dust particles. Moreover, this process also generates soot residues, which is not particularly desirable. When pyrolyzing soda lime glass, care should be taken so that moisture does not leach alkali from glass, creating sodium hydroxide residue [27]. Heating above 450 °C in ultra-high vacuum can even give rise to atomically clean surface, whereas heating only up to 100–300 °C can remove adsorbed water and various hydrocarbons.

2.2.4 *Ultrasonic cleaning*

Ultrasonic method is a relatively new addition to cleaning techniques. An ultrasonic wave is passed through a solvent kept in a stainless steel container. The transducers on the side or bottom of the tank convert oscillatory electrical input to vibratory mechanical output. Cavitation is the prime mechanism of cleaning here, as small imploding bubbles are generated with an enormous pressure of around 1000 atm, due to 20–40 kHz frequency sound waves [18]. This method is effective in removing huge chunks of stubborn materials such as polymers, resins and greases. It is routinely used in cleaning glassware in the laboratory.

2.2.5 *Laser treatment*

Laser irradiation is capable of removing contaminants and impurities from the upper layer of substrate. The mechanism of laser cleaning includes laser photodecomposition, laser ablation and surface vibration due to impact of laser pulse. Short wavelength and short pulse duration are more effective. Reports show [28] appropriate energy density is crucial for effective cleaning without causing surface oxidation and secondary contamination. Contaminants ranging

from radioactive elements to paints and dusts can be effectively removed using lasers, both in micro and large-scale applications.

Researchers have come up with optimum laser cleaning parameters such as 10 ns Q-switched Nd:YAG laser operating at 1064 nm [29] that is effective in removing burial encrustation and degradation products, without damaging the underlying substrate of excavated Greco-Roman glass. Some researchers have proposed a novel method of applying the Nd:YAG laser on the backside of the substrate submerged in water [30]. A metal plate is placed underneath the glass substrate. This metal absorbs most of the laser energy, hence vaporizes and produces turbulent bubbles that clean alumina particles of size 0.5 μm from the glass. As the laser was applied backside, the damage due to laser heat was significantly reduced.

3 Comparison of different cleaning methods

3.1 Data-wise comparison

Han et al. reported [5] a comprehensive study of glass surface cleaning using some of the common wet chemical methods. Their study showed that methods A and C (Table 2) are capable of producing comparable contact angle, roughness values and thickness loss values. Apparently piranha (method C) offers an effective cleaning method, but requires aggressive chemical conditions. On the other hand, method B produces a strong increase in surface roughness (1.66, highest in the lot). Such topology effect to the contact angle values should be even more pronounced at low CA values [34]. Both methods D and E increased the surface roughness significantly, due to the strong oxidants present in the activation solution. Method F utilizes a strong basic solution leading to the highest thickness loss in their study.

Although the comparative study by Cras et al. [4] does not report the CA values precisely, they say that methods 1, 3 and 4 in their study (Table 1) produce contact angles above 8°, whereas method 2 (methanol:HCl followed by H_2SO_4 treatment, same as method B of the previous study) shows complete wetting of the cleaned glass surface making the contact angle too small to measure (Fig. 2).

Method 4 in their investigation corresponds to RCA method, giving rise to a CA of 2° ± 2°. Acidic hydrogen peroxide solution is known to remove heavy metals from silica surfaces [2], whereas basic hydrogen peroxide removes the organic contaminants. Method 5 combines both, resulting in a higher CA of 31° ± 2°. Methods 6–8 also produced somewhat higher CA (Fig. 2) due to large intra-slide variations caused by the surface heterogeneity due to leaching and/or etching actions of the cleaning agents [35–37]. These heterogeneities would result in local curvatures of the water droplets used to make contact angle measurements, resulting in a tendency for the liquid to extend over hydrophilic areas while retreating from areas of high hydrophobicity [38].

Donose et al. [39] have effectively used lateral force microscopy to compare the changes that occur on silica surface subjected to different cleaning procedures like RCA cleaning, water plasma cleaning and UV–ozone cleaning. They found that all procedures gave comparable contact angle, surface roughness and normal force interactions. But lateral frictional forces were found to be several times higher in RCA method due to continuous generation and removal of oxide layer and hence formation of microstructures (Fig. 6).

3.2 Advantages and disadvantages

The greatest disadvantage of almost all of these glass cleaning methods is to obtain effective cleaning as indicated by the difference in contact angle, yet not to compromise surface smoothness and composition due to corrosive effect of the cleaning agent. Another biggest disadvantage is the limited number of cleaning agents that can be used in close proximity with food or ecosystems without leaving hazardous effects. And in that perspective, only some of the chelating agents qualify, examples being citric acid, glycine, tartaric acid, EDTA, etc. In-situ application also limits the usage of cleaning methods like plasma treatment or UV–ozone cleaning, as an already existing glass building or greenhouse cannot be subjected to treatment inside a chamber. Vapor degreasing leaves

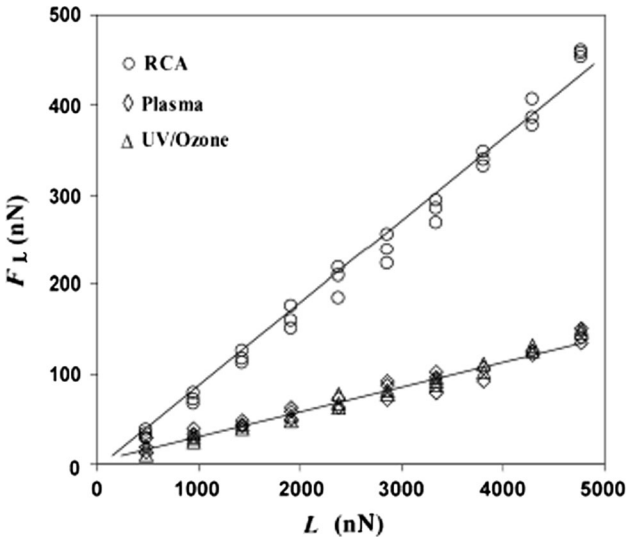

Fig. 6 Comparison of lateral force (F_L) vs. applied load (L) for the system of a 20-μm silica particle and silica wafers in water subjected to three different cleaning procedures. Reprinted with permission from [39]. Copyright: 2006 Elsevier

residual organic molecules on glass surface and causes static electricity, which is not desirable.

However, when it comes to semiconductor industry or other high-tech applications like displays and solar cells, where ecological proximity is not a concern, RCA method is the widely accepted one. The next best method of wet cleaning, as indicated in the data-wise discussion above, is the HCl–MeOH method which does not give rise to significant surface roughness or loss of substrate thickness. The remaining cleaning methods might be suitable for specific applications only.

Most of the dry cleaning techniques require sophisticated and costly instruments, although large quantity of samples can be cleaned without little or no waste generated. For example, laser treatment is extensively used to clean stained glass windows, excavated objects and archaeological artifacts due to its noninvasive nature, other advantages of this method being automation and remote control. But laser and plasma treatments may not be cost-effective in most applications.

4 Coating strategies

The concept of hydrophobicity emerges from lotus leaves. Lotus leaves typically remain clean and dry in muddy ponds. When water falls onto a lotus leaf, it beads up and then promptly rolls off the leaves, collecting dirt along the way. This behavior of self-cleaning is known as 'lotus effect'. The hydrophobicity of solid surface strongly depends upon surface energy and surface roughness. Reduction in surface energy leads to higher hydrophobicity and vice versa [40]. Literature on the basis of experiments state that surfaces with nanoscale roughness are required to form hydrophobic surfaces [41].

Some of the major coating strategies that interested us were:

1. Hydrosilylation (without native oxide layer, so HF required)
2. Silane-coupling or silanization (with native oxide layer)
3. Plasma treatment
4. DC sputtering

It should be noted that among the hydrophobic coating methods listed above, silanization strategy is capable of generating anti-reflective (AR) coating as well. Hence, special emphasis will be given to discuss this method elaborating the precursors, mechanisms, influencing factors, solvents and limitations.

4.1 Hydrosilylation

Over the past decade, there has been increasing interest in functionalizing silicon surfaces, in absence of native oxide layer. An extremely useful starting point for surface chemistry of silicon surfaces is the hydride termination, formed by short fluoride treatment, as shown in Fig. 7. Typical reagent will comprise 40 % NH_4F + 5 % HF + 55 % water, also known as buffered hydrogen fluoride (BHF) [42]. These surfaces are metastable and resistant to oxidation, yet sufficiently chemically reactive to allow for functionalization.

Researchers have shown that functionalization of silicon surface by replacing the hydrides with organic moieties is possible, as shown in Fig. 8, forming stable silicon-carbon bonds and potentially allowing for incorporation of a wide range of chemical groups. This reaction, termed 'hydrosilylation', involves insertion of an alkene or alkyne (R) into a surface Si–H bond and thus by changing the R group substituents, the characteristics of the resulting surface can be tailored at will [43].

Hydrosilylation requires initiation by UV light at room temperature or by heat, typically 120–200 °C. Since the reaction takes place only where illuminated, photo-patterning is also possible.

Another study shows [44] the effectiveness of electroless metallization of palladium, gold and copper on the hydrogen-terminated (100)-oriented single-crystal silicon surface via viologen-GMA-g-H-Si bonding where the viologen not only offers sites of reduction but adhesion promotion.

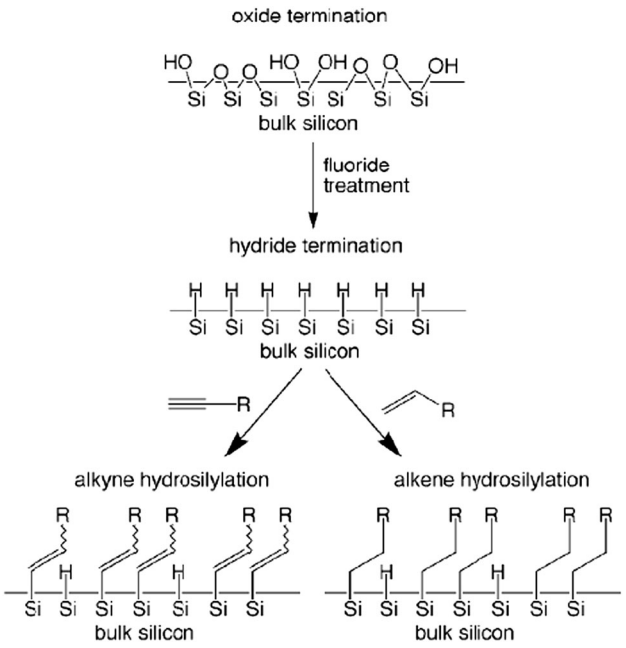

Fig. 7 Native oxide layer undergoing hydrosilylation via hydride termination. Reprinted from [43], no license required under STM agreement

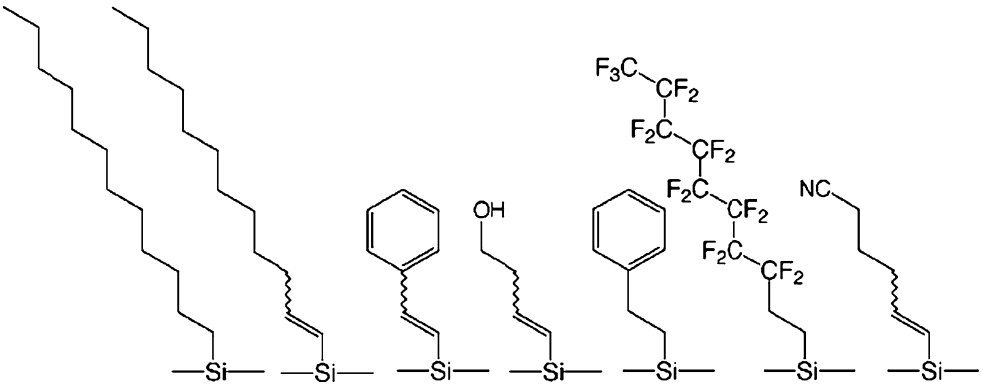

Fig. 8 Examples of some organic moieties being grafted on silicon surface through either Lewis acid-mediated or white light-promoted hydrosilylation. Reprinted from [43], no license required under STM agreement

Mechanism Stable alkyl-terminated surfaces are generated by a two-step process (Fig. 9) where the silicon surface gets chlorinated first and then a typical Grignard reaction takes place [45].

Depending on what alkene and alkyne are used, a mixed monolayer formation is also possible as shown below in Fig. 10 [45]. This accomplishes both goals of resistance to oxidation as well as of further functionalization.

4.2 Silane-coupling or silanization

Silane coupling agent is a compound with a general formula $(RO)_3$-Si-X that anchors with inorganic materials like glass or silica with the help of reactive group RO (e.g., methoxy, ethoxy etc.), whereas the reactive group X (e.g., vinyl, epoxy, amino, methacryloxy, mercapto etc.) on the other end of the molecule forms bond with organic materials like synthetic resins. In this way, a silane coupling agent is capable of bonding with both organic and inorganic surfaces and acts as an excellent adhesion promoter.

Mechanism Silane coupling reagents react with water (hydrolysis) to form silanol groups, and oligomers are formed through partial condensation. The silanol groups are then hydrogen bonded to silica (glass) surface. A final drying process may result in robust chemical bonds through dehydration-condensation reaction as shown in Fig. 11 [46].

On the other hand, a silane coupling agent is capable of improving the wettability and miscibility of the organic resin and can form chemical as well as hydrogen bonds with the resin. In this way, it acts as an adhesion promoter.

Successful and reproducible deposition of a monolayer depends not only on temperature and hydration conditions

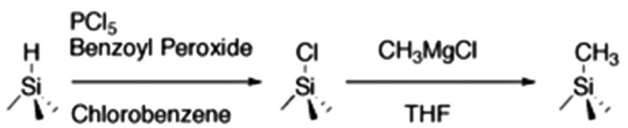

Fig. 9 Two-step chlorination-alkylation mechanism of hydrosilylation. Reprinted with permission from [45]. Copyright: Nathan Lewis

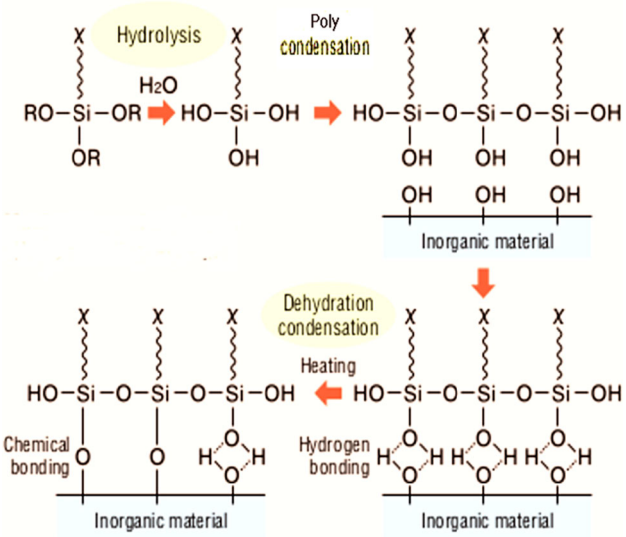

Fig. 11 Mechanism of the silanization process. Reprinted with permission from [46]. Copyright: 2011 Shin-Etsu Silicones Inc

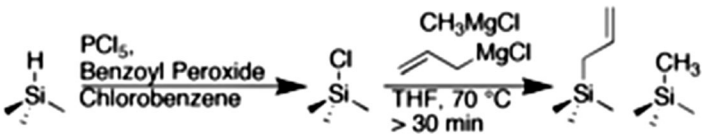

Fig. 10 Mixed monolayer formation by hydrosilylation. Reprinted with permission from [45]. Copyright: Nathan Lewis

but also on the type of silane used, packing of the chains [47–49] and the techniques employed.

4.2.1 Choice of sol–gel precursor

The hydrophilic/hydrophobic properties of the silanized particles were evaluated on the basis of wettability profiles (Fig. 12) [50]. An increase in the hydrophobicity of the modified samples were noted. The smallest mass increase, and thus the weakest affinity to water, was established for the silica modified by OPF [3-(2,2,3,3,4,4,5,5-octafluoropentyloxy)propyltriethoxysilane]. Besides, OPF significantly affected the zeta potential.

The most common silanizing agents to functionalize silica surface are the aminosilanes (e.g., APTES or 3-aminopropyl triethoxy silane, *N*-phenyl-3-aminopropyl trimethoxysilane), fluorosilanes and alkylsilanes.

Smith and Chen [51] examined the hydrolytic stability of the silane-derived layers as a function of reaction conditions and the structural features of the aminosilanes. Silane layers prepared in anhydrous toluene at elevated temperature are denser and exhibit greater hydrolytic stability than those prepared in the vapor phase at elevated temperature or in toluene at room temperature. Extensive loss of surface functionality was observed in all 3-aminopropylalkoxysilane-derived layers, independent of the number and the nature of the alkoxy groups, due to the stable cyclic intermediate. The hydrolytic stability of aminosilane monolayers derived from *N*-(6-aminohexyl)aminomethyltriethoxysilane (AHAMTES) indicated that the amine-catalyzed detachment can be minimized by controlling the length of the alkyl linker in aminosilanes.

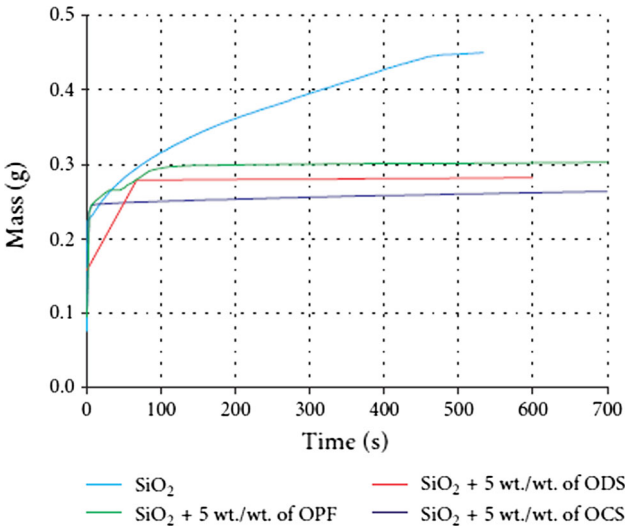

Fig. 12 Wettability profiles of modified silica fillers including the control experiment. Reprinted from [50] under Creative Commons License

However, Fiorilli et al. [52] noticed that the surface density of amino groups, as estimated through a colorimetric method, were very similar for vapor- and liquid-treated substrates, suggesting a similar reactivity and accessibility of the functional groups on the surface.

The surface properties and structure of mono-, di- and tri-aminosilane-treated glass surfaces has also been reported [53]. The positive charge characteristics of the aminosilane-modified surfaces are attributed to the formation of protonated amino groups via hydrogen bonding between amino groups and acidic OH groups on the glass surface, as revealed from the peak at 401.5 eV in the high-resolution N 1s XPS spectra. Molecular orientation study indicates a preference for protonated amino groups toward the glass surface while the free amino groups are protruding to the air-side.

4.2.2 Factors affecting

4.2.2.1 Hydrolysis conditions Water of hydrolysis may come from different sources. It may be added, it may be present on the substrate surface or it may come from the atmosphere. The degree of polymerization of the silanes is determined by the amount of water available and the organic substituent. If the silane is added to water and has low solubility, a high degree of polymerization is favored. Multiple organic substitution, particularly if phenyl or tertiary butyl groups are involved, favors formation of stable monomeric silanols. Thickness of polysiloxane layer is also dependent on the concentration of siloxane solution. It has been calculated that deposition from a 0.25 % silane solution onto glass could result in three to eight molecular layers [54]. These multilayers could be either inter-connected through a loose network structure, intermixed or both.

Glass surface modification is a pH-dependent process. The silica isoelectric point is about 2. The SiO^- concentration increases with increasing pH, allowing better interaction with aminosilane. At high pH, some of the silanol groups of aminosilane is in SiO^- form and tend to repel each other. Immobilization of aminosilane changes the interaction characteristics. Because surface silanols are more acidic than silane silanols, the interaction with surface silanol is thermodynamically favored over intramolecular interaction [55].

4.2.2.2 Bonding conditions Factors that contribute to the ability of an organosilane to generate a hydrophobic surface are its organic substitution, the extent of surface coverage, residual unreacted groups (both from the silane and the surface) and the distribution of the silane on the surface. In general, surfaces become more hydrophilic in the series: nonpolar < polar, no hydrogen-bonding < polar, hydrogen-bonding < hydroxylic < ionic [54]. The

number of sites and the structure and density of the interphase area also have significant influence on hydrophilicity.

4.2.2.3 Silanization agent Factors influencing silane surface modification include:

- Concentration of surface hydroxyl groups
- Type of surface hydroxyl groups
- Hydrolytic stability of the bond formed
- Physical dimensions of the substrate or substrate

Concentration and type of hydroxyl groups may vary widely in a substrate. Freshly fused substrates stored under neutral conditions have a minimum number of hydroxyls. Hydrolytically derived oxides aged in moist air have significant amounts of physically adsorbed water which can interfere with coupling. Hydrogen-bonded vicinal silanols react more readily with silane-coupling agents, while isolated or free hydroxyls react reluctantly [54].

In general, the reactivity of hydroxylated surfaces with organofunctional silanes decreases in the order: Si–NR_2 > Si–Cl > Si–NHSi > Si–O_2CCH_3 > Si–OCH_3 > Si–OCH_2CH_3 [54]. Bond energy analysis indicates that the formation of the Si–O-surface bond is the driving force for the reaction under dry and aprotic conditions. Secondary factors contributing to the reactivity of organofunctional silanes with a surface are the volatility of the by-products, the ability of the by-product to hydrogen bond with the hydroxyls on the surface, the ability of the by-product to catalyze further reactions and the steric bulk of the groups on the silicon atom.

4.2.2.4 Steric effect As discussed earlier, aliphatic or fluorinated hydrocarbon substituents impart hydrophobic character to the surface. Steric effect such as chain length and branching of hydrocarbon chains are equally important. Dipodal silane agents often exhibit substantial improvement in performance due to tighter network formation and hence better hydrolytic stability.

4.2.3 Choice of solvent

Solvent can play a crucial role in silanization. Hozumi et al. [56] have used strong base (NaOH) and acid (HNO_3) as post-washing solutions; however, their study and earlier studies [57–59] indicate that the loosely bounded silane molecules are easy to remove with alcohols and/or H_2O washings immediately after the silanization step.

Water content of silane solution may have profound influence on layer formation, changing from continuous growth at low water content to island growth at higher water content [60].

On the other hand, variation of solvents can influence the silanization process as well. Solvents with a high capacity for dissolving water, such as 1,4-dioxane, are not preferable for generating self-assembled monolayers of OTS on glass, as they may over-solubilize the alkyltrisilanol species and prevent polymerization onto the substrate surface. Conversely, solvents with a very low capacity for dissolving water such as n-pentane cannot supply enough moisture to the bulk phase, and little alkyltrisilanol is produced. The best quality monolayers are produced when toluene or benzene are used as solvent, because they can solubilize optimum quantity of water necessary for the formation of alkyltrisilanol species and allow the alkyltrisilanol species to polymerize onto the substrate surface without providing undue steric hinderance [61] (Table 3).

4.2.4 Limitations

Methoxy and ethoxysilanes are the most widely used organofunctional silanes for surface modification. This is because they are easily handled, and the alcohol by-products are non-corrosive and volatile. The methoxysilanes are capable of reacting with substrates under dry, aprotic conditions, while the less reactive ethoxysilanes require catalysis for suitable reactivity. This might be a limitation as far as applications are concerned. Residual (non-condensed) hydroxyl groups from alkoxysilanes may also interfere with the polylayer deposition process, posing complication.

4.3 Plasma treatment

The beauty of this method is that the same technique can be used for pre-treatment cleaning as well as subsequent hydrophobic modification. The usual process involves coating the glass surface with PDMS silicone oil. Then, the glass samples are put into the discharge chamber for plasma processing. When the process is over, the unwanted silicone oil on the treated glass surface is removed by rinsing with sodium hydroxide and acetone solution [21].

Wang and He [21] observed that the contact angle steeply increased up to 105°, i.e., the hydrophobicity increased with increase in plasma power and plasma treatment time (Fig. 13).

When plasma was employed on the glass surface covered with silicone oil, the glass surface and the PDMS molecules are exposed to high reactive regime of DBD. The energetic electrons collided with glass surface covered with PDMS oil. This may break the chemical bonds of PDMS silicone oil molecule and –OH of glass surface because their chemical bond energies are not more than 5 eV (C–H: 4.3 eV, C–Si: 2.9 eV, Si–O: 3.8 eV, O–H: 4.8 eV) [21]. The reactions among the broken bonds may produce some hydrophobic groups, such as $–CH_3$ and broken PDMS chains, on glass surface. Thus, after plasma treatment, the glass surface is hydrophobic.

Table 3 Advantages and disadvantages of common leaving groups of silanization. Adapted from [54]

Type	Advantage	Disadvantage
Dimethylamine	Reactive, volatile by-product	Toxic
Hydrogen chloride	Reactive, volatile by-product	Corrosive
Silazane (NH_3)	Volatile	Limited availability
Methoxy	Moderate reactivity, neutral by-product	Moderate toxicity
Ethoxy	Low toxicity	Lower reactivity

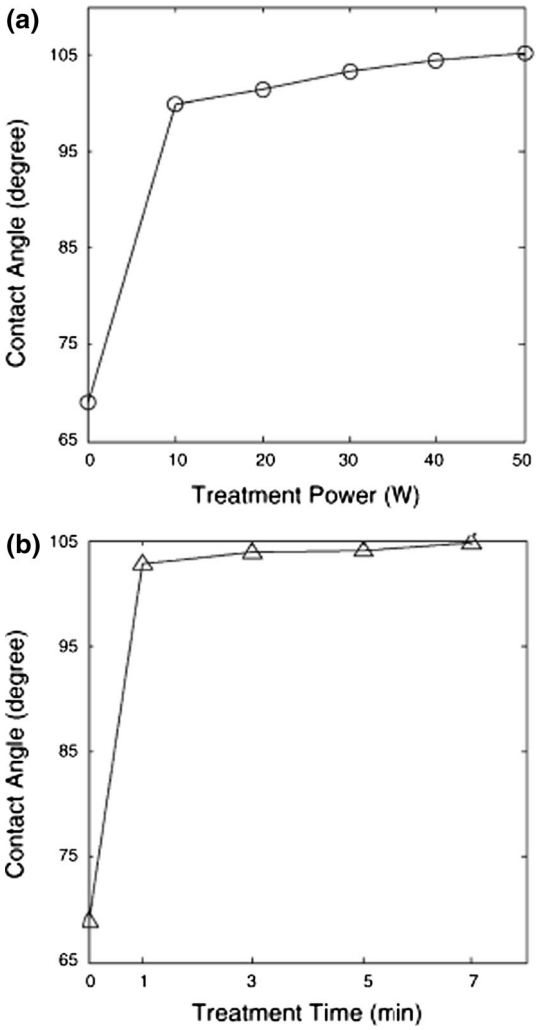

Fig. 13 **a** Change in contact angle with treatment power (treatment time = 15 s). **b** Change in contact angle with treatment time (treatment power = 50 W). Reprinted with permission from [21]. Copyright: 2006 Elsevier

4.4 DC sputtering

V. Dave et al. [62, 63] have recently come up with a unique hydrophobic coating made of Hafnium oxide which has high dielectric constant, large band gap (5.6 eV), high refractive index (2.1) and good mechanical, thermal and chemical properties. They used DC magnetron sputtering technique and found out a magnetron pressure of 15 mTorr (Fig. 14) and a DC power of 60 W to be optimum for highest crystallite size (giving rise to less dislocation and grain boundaries), highest hydrophobicity as evident from high contact angle (102.3°), highest surface roughness (4.8 nm), highest film thickness (865 nm) due to lowest packing density 0.88, highest extinction coefficient (0.41), and hence least transparency (90 %) due to max grain size, i.e., highest scattering; as evident form contact angle and semi-contact AFM measurements, respectively.

Uniform coating, reproducibility, controllable growth, high deposition rate and low contamination effect are some of the advantages of reactive magnetron sputtering [64].

5 Instrumental techniques

5.1 Contact angle

As discussed earlier, contact angle (CA) is a measure of surface hydrophobicity. An equilibrium CA greater than 90° indicates hydrophobicity, whereas an equilibrium CA less than 90° indicates hydrophilicity (Fig. 15a). The native oxide layer on silicon comprises lots of silanol group which makes the surface hydrophilic. Gradual depletion of silanol groups by long-chain alkyl groups and formation of siloxane bonds (–Si–O–Si–) can switch the nature of the surface to hydrophobic.

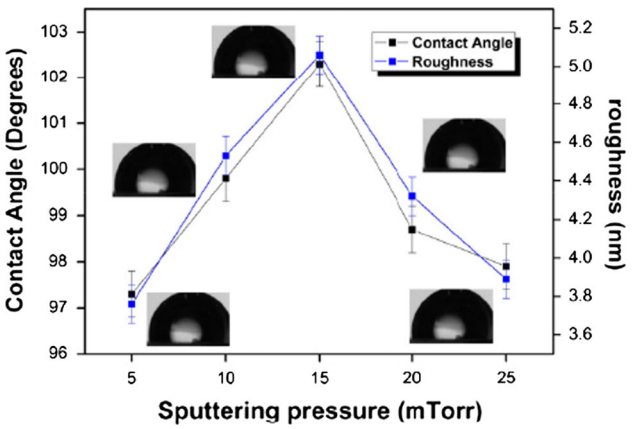

Fig. 14 Variation of contact angle and roughness as a function of DC sputtering pressure. Reprinted with permission from [63]. Copyright: 2013 Elsevier

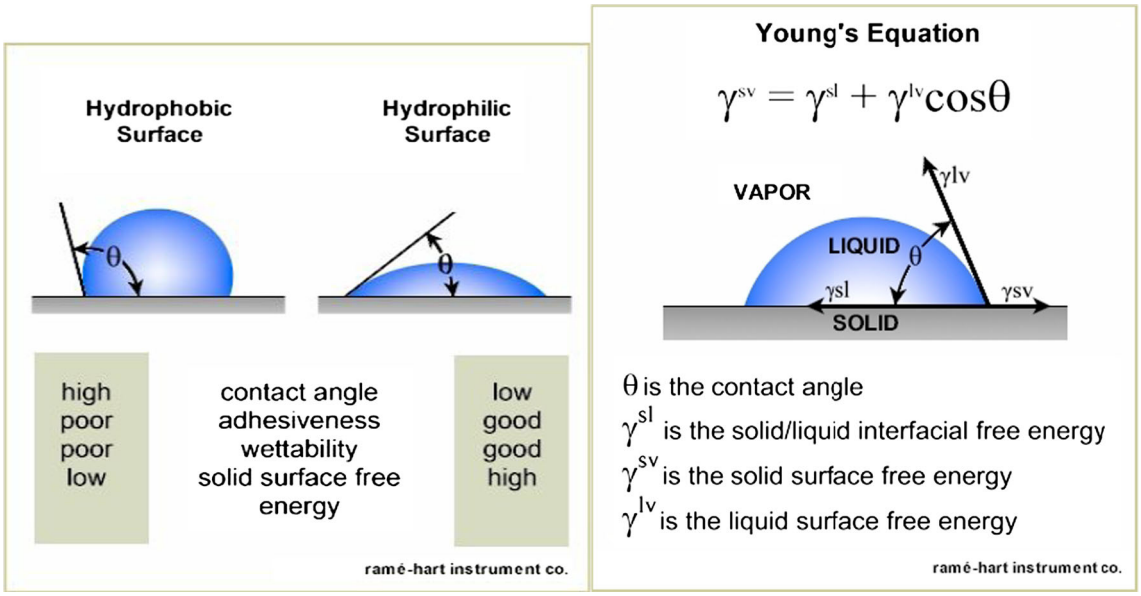

Fig. 15 **a** Contact angle of hydrophobic and hydrophilic surfaces **b** Young's equation correlating contact angle to surface energies (Reprinted with permission from : Ramé-hart Instrument Co.)

Changes in surface topology might additionally influence the CA results. The surface roughness can be quantified by using the root mean square (RMS) value R_q and the surface area difference (SAD). R_q represents the root mean square average of height deviations Z_i taken from the mean data plane (Eq. 1).

$$R_q = \sqrt{\frac{\sum Z_i^2}{n}} \tag{1}$$

The SAD is defined as the difference between the three-dimensional surface area and its two-dimensional projection SAD = 1 − A3D/A2D. The SAD provides a measure for the effective surface area of the solid–liquid contact [5]. This aspect is of particular interest for the electrical characterization, especially for the calculation of the interface capacitance of the sensor chips.

Literature shows that sessile drop profiles can be fitted through the Young–Laplace method (Fig. 15b), and the contact angles between fitted function and base line can be calculated [52]. Surface free energy of both the bare and the functionalized substrates was determined using the method by Owens and Wendt [65]. These authors developed the idea that both the solid superficial energy and the liquid surface tension can be separated into two terms: (1) a polar contribution due to Coulomb interactions between permanent or induced dipoles and (2) a dispersive contribution due to van der Waals forces.

$$\sigma_l = \sigma_l^d + \sigma_l^p \quad \text{and} \quad \sigma_s = \sigma_s^d + \sigma_s^p \tag{2}$$

where σ_l^d and σ_l^p represents the dispersive and polar parts of the liquid, respectively, and σ_s^d and σ_s^p represents the respective dispersive and polar contributions of the solid. The interfacial energy from the contributions of the liquid and solid ($\sigma_{s,l}$) is given by

$$\sigma_{s,l} = \sigma_s + \sigma_l - 2\left[\sqrt{\left(\sigma_s^d \sigma_l^d\right)} + \sqrt{\left(\sigma_s^p \sigma_l^p\right)}\right] \tag{3}$$

Taking into account Young's formula (from the equilibrium of the forces at the edge of a drop on a solid surface),

$$\sigma_s = \sigma_{l,s} + \sigma_l \cos\theta \tag{4}$$

one can obtain an equation of the form

$$y = ax + b, \text{ with } y = \frac{1+\cos\theta}{2}\frac{\sigma_l}{\sqrt{\sigma_l^d}}, \; x = \sqrt{\frac{\sigma_l^p}{\sigma_l^d}}, \quad a = \sqrt{\sigma_s^p}, \text{ and } b = \sqrt{\sigma_s^d}. \tag{5}$$

Here, both parameters x and y depend only on the liquid, and the parameters a and b depend only on the solid. Considering a series of different liquids, plotting of y versus x allows one to calculate σ_s^p from the slope of the fitted line and σ_s^p from the intersection with the y axis.

5.2 SEM and AFM

AFM should be used in non-contact or tapping mode to avoid sample damage during measurement. A post-silanization rinsing with methanol for 5 min is sometimes effective to remove weakly bound physisorbed molecules and thus to obtain a smooth coated surface. This can be confirmed by AFM images that reveal formation of 'silane

islands' [53] in unrinsed samples after APTES coating. Another interesting fact is that although plasma cleaning is capable of taking off the dusts, grease and other impurities, it causes increase in surface roughness which is supported by mountain-like features seen by AFM, the number of these features increasing with treatment time (Fig. 16) [21].

Microstructure formation in sol–gel films depend on the relative rates of hydrolyzation and condensation. In acid-catalyzed sol–gel process, the hydrolysis is fast and the condensation is slow, giving rise to dense and smaller pore volumes. On the other hand, in base-catalyzed condition, hydrolysis is much slower than condensation which results in much larger and loosely held pores (Fig. 17) [66]. Thus, base-catalyzed coating gives better anti-reflectance property due to larger pore size, but acid-catalyzed coating gives much stable bonding with substrate and better abrasion resistance property [67]. Another difference is that base-catalyzed process requires a reflux step at 80 °C, which is not required in acid-catalyzed process making it suitable for various in situ applications. Besides, as far as storage and aging of sol is concerned, the acid-catalyzed sols are relatively much more stable with a shelf life of 1 year. Researchers often combine acid-catalyzed and base-catalyzed processes to achieve the advantages of both.

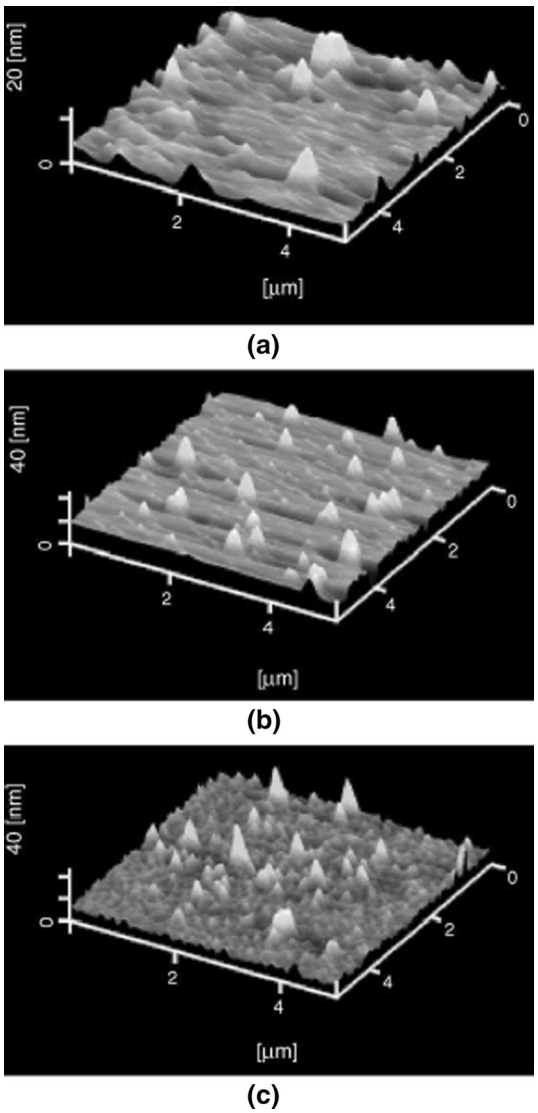

Fig. 16 AFM images of plasma-treated glass samples: **a** control **b** 1 min treatment **c** 5 min treatment. Reprinted with permission from [21]. Copyright: 2006 Elsevier

Figure 18 shows the microstructure of base-catalyzed sol–gel coating which is further made superhydrophobic by immersing the coated surface in 10 % TMCS (trimethylchlorosilane) solution in hexane. The figure shows how the microstructure changes with TMCS treatment time and proposes an optimum time of 24 h [68]. A balance between inter-particle porosity and surface roughness is the key in achieving simultaneous anti-reflective hydrophobic coating.

5.3 XPS

XPS is a powerful surface analytical technique for determining elemental composition, empirical formula, and valence states. The electron emission angle determines the surface sampling depth. Researchers have [52] collected O 1s, N 1s, C 1s and Si 2p core levels of silanized surfaces, referencing all core-level peak energies to saturated hydrocarbon peak at 285.0 eV. Some instruments can be equipped with consistent charge compensation unit even at near-grazing take-off angles [53].

5.4 Ellipsometry

Ellipsometry is a widely used technique for obtaining the layer thickness of different surfaces, based on refractive index measurement. Combining XPS data with ellipsometric study, researchers have shown [53] that the nitrogen content of atom % corresponds roughly to a monolayer of silane coverage of 7–10 Å (contrasted to the length of fully stretched APTES molecule which is 9 ± 1 Å) and the surface N content increases with APTES layer thickness and finally levels off as it approaches saturation within the analysis depth of the XPS (Fig. 19).

5.5 Zeta potential

Modification with silane leads to the introduction of new chemical groups on the silica surface, which changes its initial properties and also the surface charge, manifested by the values of zeta potential. Electrokinetic potential of unmodified silica is negative in the entire pH range studied, and the isoelectric point (IEP) was reached at pH close to 2 (precisely 1.7).

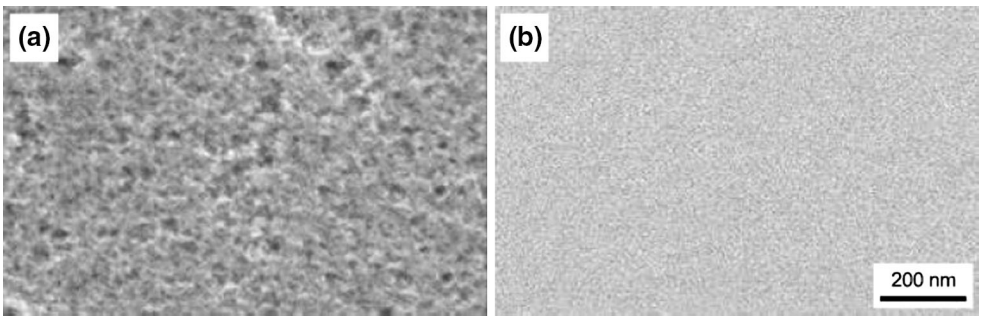

Fig. 17 Difference in porosity and surface morphology of **a** base-catalyzed and **b** acid-catalyzed sol–gel coatings. Reprinted with permission from [66]. Copyright: 2007 Elsevier

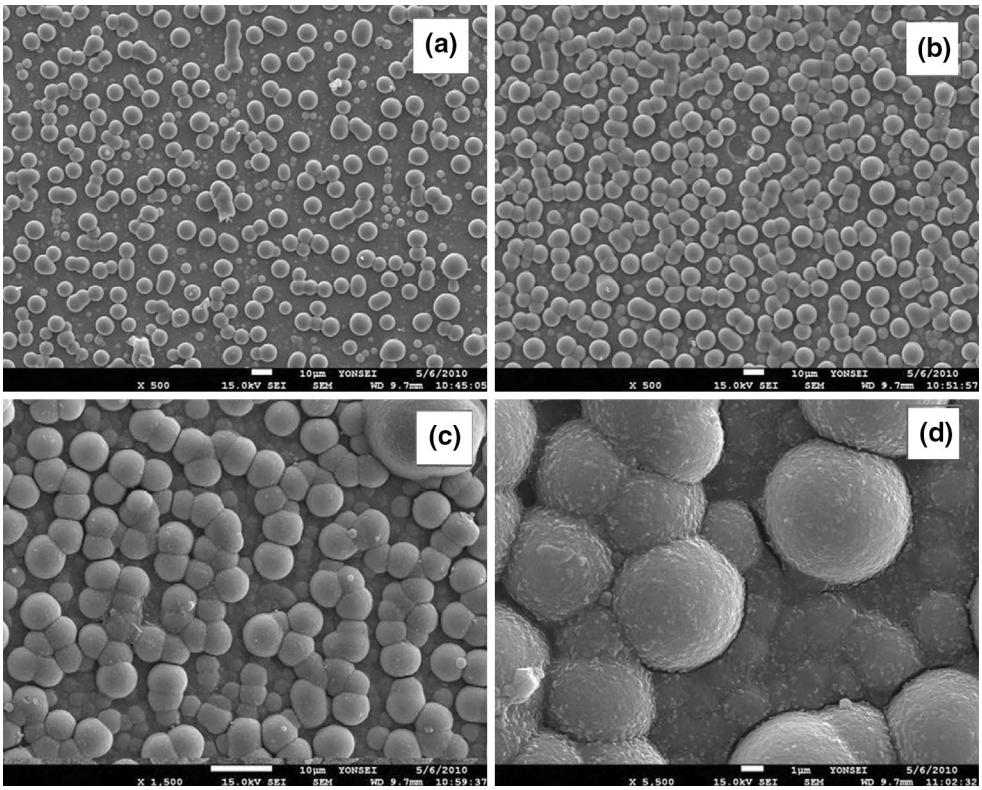

Fig. 18 FESEM images of base-catalyzed superhydrophobic sol–gel coating as a function of immersion time in 10 % TMCS solution: **a** 15 h **b** 20 h **c** 25 h **d** 25 g (5500×). Reprinted with permission from [68]. Copyright: 2010 Elsevier

Aptekar et al. [69] took three different silanization agents namely (APTES) and a 1:2 mixture by volume of APTES with bis-(triethoxysilyl)ethane (BTEOSE) or (3-trihydroxysilyl)propyl methylphosphonate (THPMP) as well as a control experiment containing no silanization agent. A change in the sign of the surface charge or zeta potential was quite evident from their experiment upon silanization, the magnitude of positive charge depending on the total amount of amine groups present, whereas the control showed negative zeta potential (Fig. 20).

Point of zero charge (PZC) is the pH value where the water contact angle has a maximum value, for example bare glass has a PZC of 3 [70]. It can be shown mathematically that [70] surface charge of APTES-treated glass leads to formation of an electrical double layer, comparable to a capacitor, when placed in contact with water. Different silanization agents will show different charge behavior.

5.6 Raman or FTIR

FTIR provides information on presence and physical interaction of functional groups. Kaolinite is a commonly used filler material that contains silica. Researchers have investigated

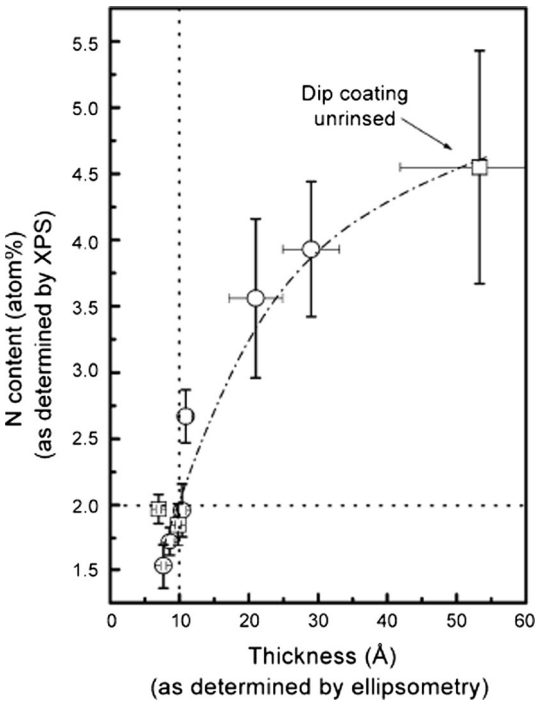

Fig. 19 The thicknesses of silane layer (by ellipsometry) on Si wafer substrate (covered with 40 ± 0.5 Å SiO_2 layer) versus the surface N content (by XPS), (*open circle*) pulsed CVD-coated, (*open square*) dip-coated samples. Reprinted with permission from [53]. Copyright: 2006 Elsevier

[71] the bonding mechanisms of silane coupling on silica surface with the help of FTIR using diffuse reflectance (DRIFT) technique.

They used different silanization agents namely *N*-(2-aminoethyl)-3-amino-propyltrimethoxysilane (Z-6020), *N*-(2-(vinylbenzyl-amino)-ethyl)-3-aminopropyltrimethoxysilane (Z-6032) and 3-glycidoxy-propyl-trimethoxysilane (Z-6040). Although OH-stretching vibrations are difficult to identify due to broad water absorption band, all of them showed a FT Raman peak at 1000 cm^{-1} assigned to Si–O–Si vibrations indicating that the polymerization has occurred in water medium (Fig. 21). A decrease in the absorbance of the C–H stretching peaks when washed with water and smaller decrease when washed with acetone indicated that no covalent bonds are being formed. Rather, hydrogen bonds are formed between the silanol hydroxyl groups and the hydroxyl groups on the kaolinite edge surface. They proposed that the oligomers are bonded to the kaolinite surface by hydrogen bonding only and that no covalent bonds are present [71].

5.7 ToF–SIMS

The wettability of the surfaces was first of all studied by Young [72] by proposing a minimization model of three phase interfacial energies solid–vapor (sv), solid–liquid (sl) and liquid–vapor (lv) through the following equation

$$\cos\theta_w = \frac{\gamma_{sv} - \gamma_{sl}}{\gamma_{lv}} \quad (6)$$

where θ_w is the Young water contact angle. If $\theta_w > 90°$, surface is hydrophobic, else hydrophilic. This work was further extended by Wenzel by associating the concept of roughness with hydrophobicity.

According to the Wenzel model [73] the apparent contact angle for a rough surface is given by:

$$\cos\theta = r\cos\theta_b \quad (7)$$

where θ_b is a contact angle on a smooth surface which depends on the interfacial energies of three phases in contact and r is a surface roughness factor. The roughness factor is defined as the ratio of true area to that of projected area [74]. The roughness factor affects the hydrophobicity via changing the roughness. According to Wenzel's equation, after enhancing the roughness of a solid surface, a hydrophilic surface ($\theta_b < 90°$) becomes more hydrophilic ($\theta < 90°$) and a hydrophobic surface ($\theta_b > 90°$) becomes more hydrophobic ($\theta > 90°$).

Cassier–Baxter also studied the hydrophobicity and submitted the following Eq. [75]

$$\cos\theta_r = f_1\cos\theta - f_2 \quad (8)$$

where θ_r and θ are the contact angles for rough and smooth surfaces, respectively, f_1 and f_2 are the fractional interfacial areas of solid/liquid and air/liquid. Apparently, a larger air/liquid fraction f_2 yields a more hydrophobic surface. It was reported that the wettability of a surface can be enhanced by increasing the surface roughness because the air trapped between the solid surfaces and the water droplet can minimize the contact area. Thus, the structures which are rough at nanoscale are the most promising surfaces from hydrophobicity point of view [76].

6 Anti-reflective (AR) and transmittance properties

Glass coatings have been studied and currently employed since the second half of the 20th century. Coatings can modify the surface properties of glass, aiming to optimize visual transmittance (antireflective coatings), thermal transmittance (low-E coatings), solar factor (solar control filters) and glass maintenance (self-cleaning coatings). Combined with the statistical amount of world glass production of almost 10^9 m^2/year [77], this can be quite significant. The use of high-performing glass in building envelopes (buildings, greenhouses, etc.) often times referred as third skin, can play an active role. The future lies in

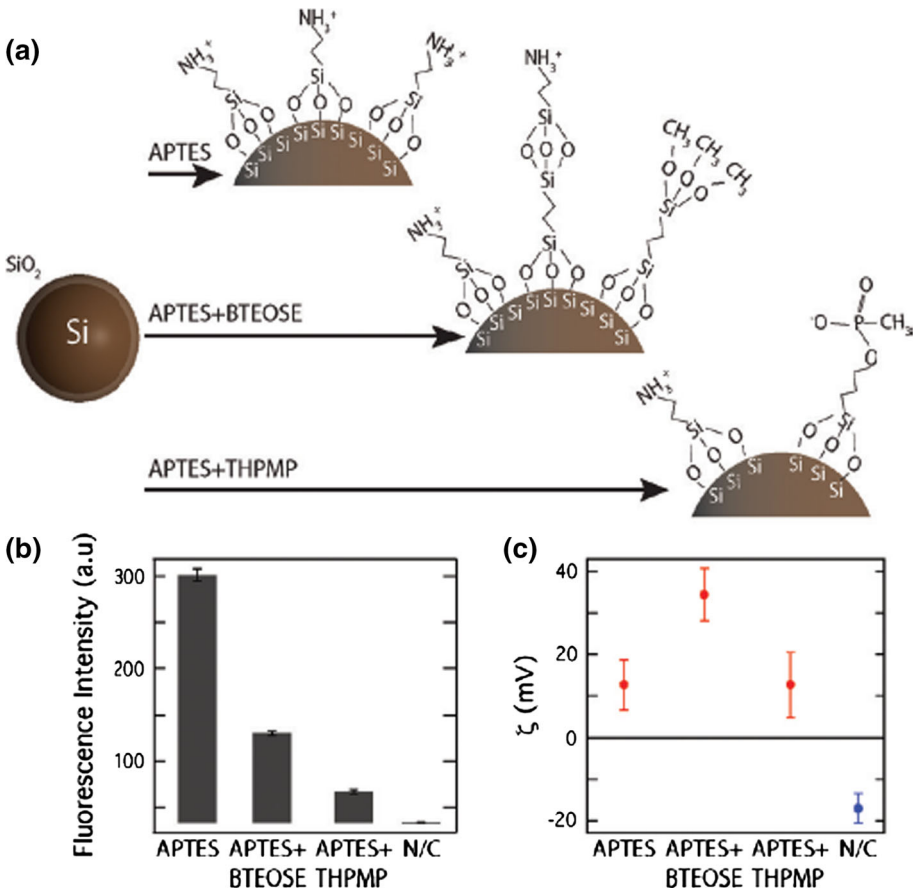

Fig. 20 Amination of silica nanoparticle by 3-aminopropyl)triethoxysilane, APTES as well as 1:2 mixture by volume of APTES with bis-(triethoxysilyl)ethane (BTEOSE) or (3-trihydroxysilyl)propylmethylphosphonate (THPMP): **a** Schematic of the process **b** fluorescence before and after silanization **c** zeta potential before and after silanization. Reprinted with permission from [69]. Copyright: 2009 American Chemical Society

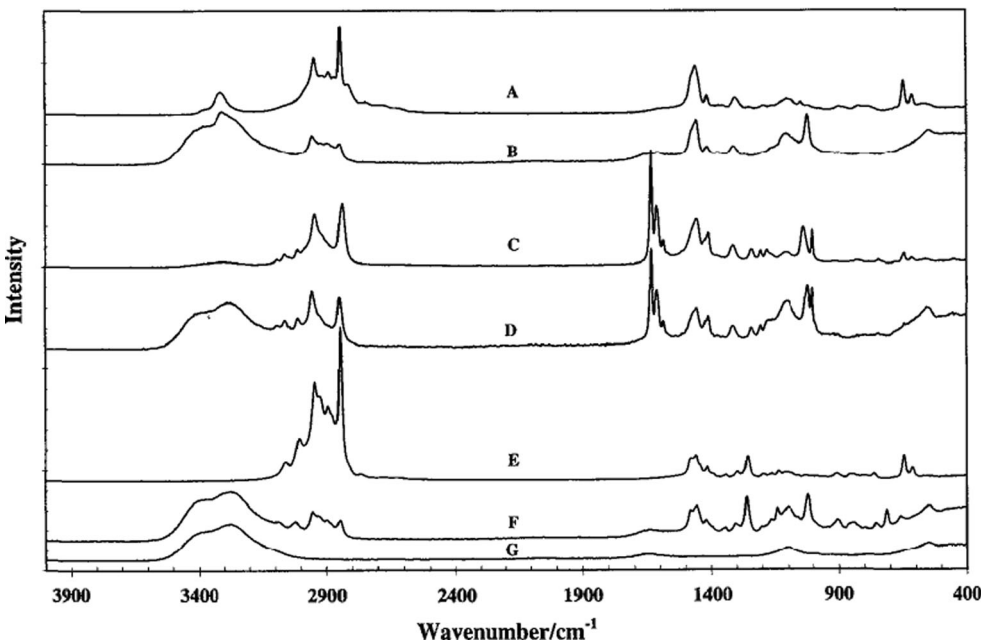

Fig. 21 FT Raman spectra of: (*a*) *N*-(2-aminoethyl)-3-aminopropyl-trimethoxy silane, Z-6020 (*b*) Z-6020 in water (*c*) *N*-(2-(vinylbenzylamino)-ethyl)-3-amino-propyltrimethoxy silane, Z-6032 (*d*) Z-6032 in water (*e*) 3-glycidoxy-propyltrimethoxy silane, Z-6040 (*f*) Z-6040 in water and (*g*) water. Reprinted with permission from [71]. Copyright: 1999 Mineralogical Society of Great Britain and Ireland

tailoring the properties without compromising the features which can be done with the help of nanotechnology and biomimetics.

6.1 Principle of AR coating

In the last few years, the development of novel anti-reflection sol–gel coatings has attracted great interest. In order to shift the reflectance to a minimum value, a fine control of the coating thickness and refractive index is required [78, 79].

The reflective loss of an optical surface is related to the difference between the refractive indices of environment and the optical material. Each time a beam comes in contact with an air–glass interface, there is the opportunity for losses in transmission (called Fresnel losses) due to the difference in refractive indices of the air and glass. Fresnel loss accounts for roughly a 4 % transmission loss for each air/substrate interface [80]. By depositing a coating on the substrate surface, the difference in refractive indices between the coating and the air is decreased, which helps to maintain maximum transmission.

For good antireflection properties, a coating must satisfy two conditions that lead to complete destructive interference [80].

1. The phase condition: for destructive interference of the reflected beams, the optical thickness (n_c h_c) of the layer must be at least a quarter of the wavelength of the incident wave. This quarter-wave condition gives the ideal thickness of the coating:

$$\lambda_0 = 4 n_c h_c \tag{9}$$

   where λ_0 is the wavelength at which destructive interference occurs.
2. The amplitude condition: for complete destructive interference, the amplitudes of light reflected from the coating-air and substrate-coating interfaces have to be equal. This condition is satisfied when the refractive indexes of the coating (n_c), the environment (n_e) and the substrate (n_s) are given by the following relation:

$$n_c = (n_e n_s)^{1/2} \tag{10}$$

If air is the environment ($n_e = 1$) then $n_c = \sqrt{n_s}$). Nearly zero-reflectance can be reached, if this condition is met. The lowest refractive indices for dielectrics are on the order of 1.35 (CaF_2, MgF_2). Therefore, sol–gel AR coatings must present index values within the range of 1.21–1.25, which is lower than that of any known solid material.

There are two approaches to produce graded refractive index coatings [80]. One is to pattern the substrate surface with a sub-wavelength periodic structure (Fig. 22a), and the second is to use a nanoporous coating (Fig. 22b).

In the first case, the refractive index of the inhomogeneous layer decreases gradually from n_s to unity. The optical properties of such a sub-wavelength-structured surface are explained by considering that the surface structure acts as a periodic diffraction grating. If the period of the grating ($\lambda_{structure}$) is small compared to the wavelength of light, only the zero-order diffracted wave propagates and higher diffraction orders are suppressed [81, 82].

In the second case, as the refractive index of a material is related to its density, by introducing porosity or layers, its value can be dramatically reduced. The relationship between refractive index and porosity is depicted by the equation

$$n_{pc} = \left[(1 - P/100) \left(n_{dc}^2 - 1 \right) + 1 \right]^{1/2} \tag{11}$$

where n_{pc}, n_{dc} and P are the refractive indexes of porous and densified coatings, and the porosity percentage, respectively [83]. To reduce the refractive index to up to $\sim$1.23 using the material with a refractive index of $\sim$1.5, the porosity of $\sim$60 % has to be introduced [84]. In order to prevent scattering, homogenous pore distribution, pore size noticeably smaller than the wavelength of light (i.e., mesoporosity: 2–50 nm), and nanometric particle sizes are required. Base-catalyzed sol–gel processes (e.g., Stöber process) [85, 86] or use of removable templates [87] have shown to be suitable synthetic routes to prepare AR coatings that satisfy the later requirements.

Various approaches to tune porosity, such as a multilayer structure with layers of varying refractive indices, a surface-relief structure made by phase separation, selective dissolution, lithographic patterning technologies, homogenous porous coatings prepared by sol–gel processes [88] and layer-by-layer assembly of deposited nanoparticles have been reported.

The following section will elucidate the methods and properties of obtaining nanoporous sol–gel coatings on glass, which relies on the basic principle of silanization as discussed in Sect. 4.2. The key to obtain simultaneous antireflective as well as hydrophobic coating is to make bilayer structure where the bottom layer will be anti-reflective due to optimum porosity and the top layer will be hydrophobic due to some extent of roughness incorporated through trimethylchlorosilane treatment [89].

6.2 Methods of generation of AR coating

6.2.1 Water-based manufacturing of AR coating

This process is 100 % environment-friendly because the experimental procedure is based on water-soluble

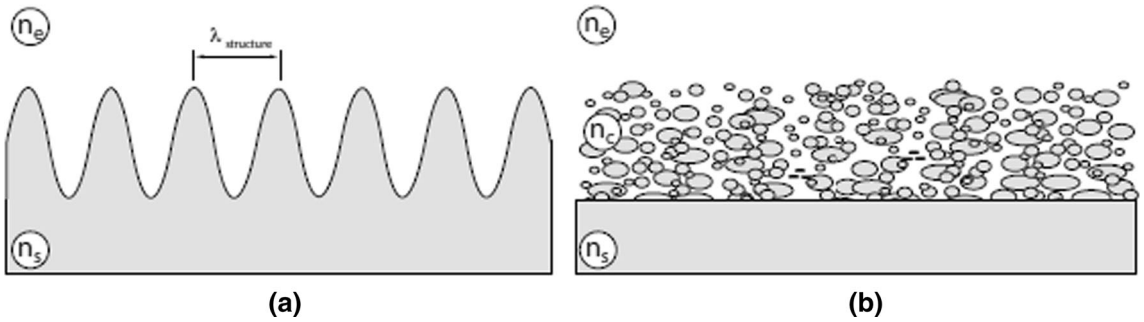

Fig. 22 Two approaches of using inhomogeneous layers as anti-reflective coating **a** Moth-eye type **b** nanoporous type. Reprinted from [80]

components. Researchers [80] have produced a SiO_x solid network starting with the precursor 'Natron Water Glass' ($Na_2Si_3O_7$). The structure of the SiO_x network was formed by controlling the condensation of small primary silica particles (polymeric or colloidal) with a diameter of a few nanometers. These particles are dispersed in a liquid, forming a so-called sol. Increasing the particle number and sizes increases the density of the sol. Eventually, the particles start to touch each other, forming a sponge-like three-dimensional network, called gel.

By stopping the process at the sol state, it is possible to spin-coat the solution. To form the sol, acetic acid was added to an aqueous solution of sodium silicate (water glass):

$$\begin{aligned} &Na_2SiO_3 + \ CH_3COOH \ + H_2O \\ &\quad = [SiO_2 \cdot nH_2O] \ + \ 2Na^+COOH^- \end{aligned} \tag{12}$$

The chemical reactions during the sol–gel process are described by three equations

$$\begin{aligned} -Si-OR + H_2O \ + \text{acid or base} &= -Si-OH + \ ROH \\ -Si-OH + \ HO-Si- &= -Si-O-Si + H_2O \\ -Si-OR + HO-Si- &= -Si-O-Si + ROH \end{aligned} \tag{13}$$

The first equation in Eq. (13) defines the hydrolysis process, while the other two defines the condensation process. Both processes are strongly influenced by the concentration of the components, the nature of solvent, the temperature and the pH of the solution. In this method, due to the acidic conditions (pH: 2–5) hydrolysis was favored [80]. A large number of monomers and small oligomers with reactive Si–OH groups were formed. These molecules reacted with each other forming the sol solution. Adding an organic polymer (10 % polyacrylamide or PAA) to the sol solution, resulted in a phase separation between the inorganic and the organic phases when evaporating the solvent. The subsequent removal of the organic phase resulted in a porous silica film. A pore size of 50 nm in diameter was achieved by varying the amount of the polymer and the sol particles [80].

6.2.2 AR coating prepared from TMOS precursor

The second method for preparing hard AR coating makes use of tetramethoxysilane $Si(OCH_3)_4$ alkoxide as precursor and poly(methyl methacrylate) or PMMA as organic component. The sol phase was prepared by polymerizing tetramethoxysilane (TMOS) monomers in an acidic environment, using hydrochloric acid (HCl) as catalyst. Hydrolysis and polycondensation reactions occurred when water and catalyst were added to the precursor [90–96]. The hydrolysis reaction is:

$$Si(OCH_3)_4 + \ H_2O \ + HCl = [SiO_2 \cdot H_2O/CH_3OH] \tag{14}$$

The condensation reactions are:

$$\begin{aligned} &\text{(alcoxolation)} \\ &(OCH_3)_3-Si-OH + HO-Si-(OCH_3)_3 \\ &\quad = (CH_3O)_3-Si-O-Si-(OCH_3)_3 + \ CH_3OH \\ &\text{(oxolation)} \\ &(CH_3O)_3-Si-OH + HO-Si-(OCH_3)_3 \\ &\quad = (CH_3O)_{x-1}-Si-O-Si-(OCH_3)_3 + \ H_2O \end{aligned} \tag{15}$$

The two chemical processes take place simultaneously in the sol–gel process. The sol solution was subsequently mixed with a PMMA solution and spin-coated onto the substrate. After removing the PMMA, a porous layer with high-quality AR properties was obtained [80].

6.3 Transmittance properties

Stober's method is quite well known for synthesizing mono dispersed colloidal silica nanoparticles. This is done by hydrolysis of a silicon alkoxide precursor, tetraethylorthosilicate (TEOS), in ethanolic medium and in the presence of ammonia, utilizing a sol–gel method. One of

the main advantages of the sol–gel process is the easy deposition of thin films directly from the solution by techniques such as dip-coating, spin-coating or spray technique [84]; dip coating being the most popular one where the nanoparticles self-assemble, as the colloidal suspension is withdrawn by evaporation [59].

Various inter-related factors can play a role in the final physical properties of sol–gel-derived coatings: (1) sol–gel solution (starting chemicals, sequence of mixing, concentration and ratio of components, temperature, pH); (2) method of application (dip, spin, spray, laminar flow); (3) substrate (glasses, plastics, metals, ceramics) and its surface conditions; and (4) coating (porosity, residual OH, structure, roughness, thickness). Variation of AR behavior with SiO_2 sol concentration, deposition rate, coating time and temperature has been reported in literature [84].

6.3.1 *Effect of deposition rate and sol concentration*

Literature shows [84] that the intensity of transmission increases with increasing the immersion rate from 5 mm/min (97.5 %) to 40 mm (99.7 %) (Fig. 23). Besides, the transmission maximum is shifted from 380 nm to longer wavelength. Thus, the changes in the deposition rate resulted in the changes of the coloration of the reflected light from the coating, ranging from a blue tint to a yellowish tint as the deposition rate decreased. They also noted the best AR behavior for 3 % SiO_2 sol, out of 2, 3 and 5 % concentration range.

6.3.2 *Effect of temperature*

It is also reported [84] that reflectance spectra of samples remained unaffected by the temperature change, although the minima shifted toward longer wavelengths with increase in temperature (Fig. 24). This kind of silica AR coating is prone to laser damage which can be an issue for high peak-power laser optics application which can also be optimized through sol–gel method [84].

6.3.3 *Effect of film thickness*

Literature also shows that [80] both $Na_2Si_3O_7$- and TMOS-based preparation methods result in porous silica layers with increase in the optical transmission through the glass substrates in the visible wavelength range to $T \approx 99$ %. Thickness of AR layer can be adjusted by varying rotation speed, which in turn will cause a shift in transmission maxima; however, AR properties remain unchanged by change in angle of incidence.

Researchers have used a triblock copolymer surfactant, Pluronic F127, to template the AR coating [97]. They noted that the value of the maximum transmittance decreases as it shifts to longer wavelengths with increase in TEOS:EtOH ratio and film thickness (Fig. 25). This is probably due to good match between optimized refractive index and thickness. They also showed that a TiO_2 interference monolayer caused noticeable reduction in refractive index (2.33 and 1.57 at 590 nm) and hence improved transmittance.

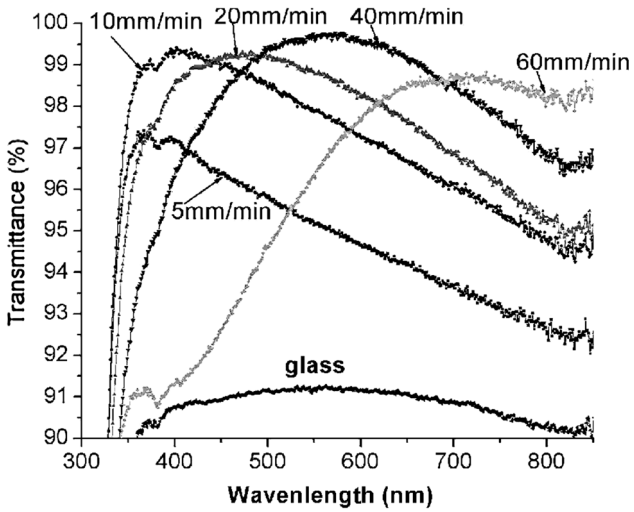

Fig. 23 Transmission spectra for silica coating on glass substrates obtained from 3 % SiO_2 using various deposition rates. Reprinted with permission from [84]. Copyright: 2007 De Gruyter Open

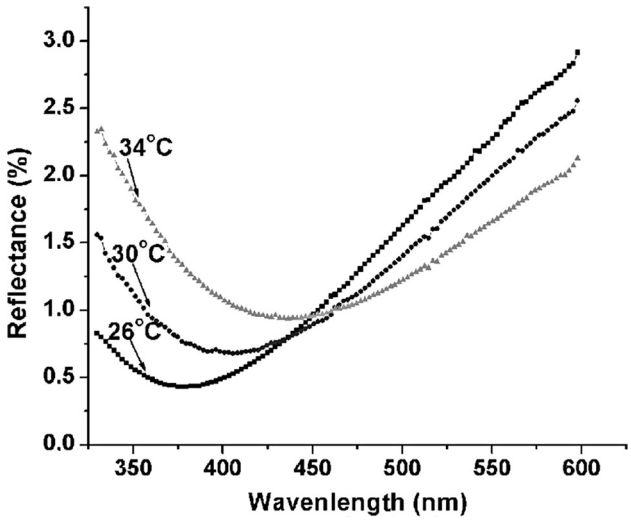

Fig. 24 Reflectance spectra for glass surface coated with silica at various temperatures. Reprinted with permission from [84]. Copyright: 2007 De Gruyter Open

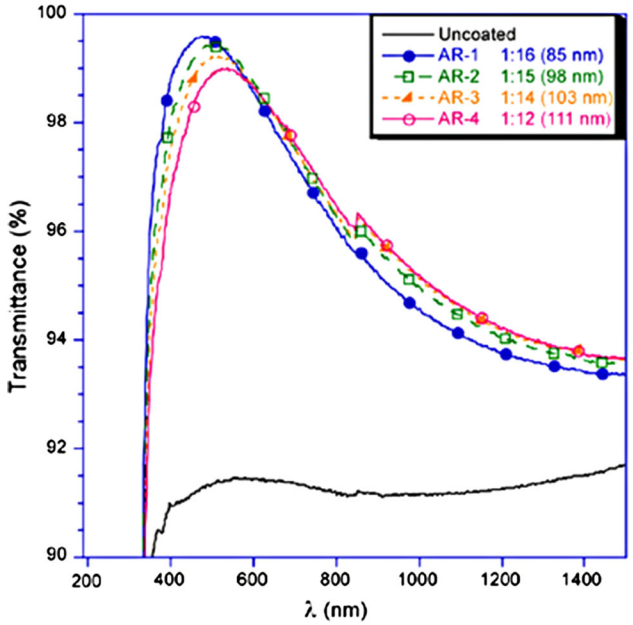

Fig. 25 Transmittance spectra for uncoated glass and coated anti-reflection samples indicating TEOS:EtOH ratio and film thickness. Reprinted with permission from [97]. Copyright: 2010 Elsevier

6.3.4 Effect of precursor

The advantage of the TMOS-based technique compared to the $Na_2Si_3O_7$ coating is its better applicability on an industrial scale. The $Na_2Si_3O_7$ coating solution in water was very unstable due to the short time needed for gelation process to take place (30 s vs. 3 h) [80]. However, the reaction could be somewhat stabilized by changing the amount and the nature of the acid.

6.3.5 Effect of particle size

AR properties of electrostatically deposited L-b-L layers of polyelectrolyte and silica nanoparticles have also been studied in terms of nanoparticle (NP) size and density. Researchers found [88] that the minimum reflectance is independent of the particle size if surface NP density is held constant, and 120-nm particles are more suitable for AR design in the wavelength range of visible light (400–800 nm).

However, in contrary to previous investigations they found that too high or too low soaking time will result in increased reflection. They also conclude that it is inappropriate to consider a NP coating entirely as a homogenous porous layer. Calcination may, however, cause shrinkage in NP size, leading to increase in refractive index.

6.3.6 Effect of cross-linking

Some researchers [98] have also reported that colloidal silica particles modified by 3-Methacryloxypropyltriethoxysilane (MOTOS) and further cross-linked with each other by pentanedithiol (2:1 molar ratio of organosilane to dithiol) showed remarkable increase in abrasion resistance as monitored by dry wipe test, yet decrease in transmittance properties. Cross-linkers like propanedithiol and butanedithiol did not influence the transmittance properties at all. Mechanism for such observation remains unexplained.

7 Applications

During the last years, the development of novel anti-reflection sol–gel coatings has attracted great interest, mainly due to their relatively low cost and to their potential application on a variety of commercial purposes, such as solar thermal collectors, solar cells, architectural glasses, windscreens, high power lasers and video display panels [97].

Thin films of functional organosilane molecules on solid surfaces have found important industrial applications, such as supports for biomolecules and catalysts, advanced composite materials, and synthesis of chromatographic supports [53]. Silanization of glass slides or silicon oxide surface finds use in biosensor development for example immobilization of biomolecules like enzymes, proteins and DNAs [5]. Glass surface composition, organofunctionalization and other monolayer coatings can be used to control reactivity from passive to active. These systems find use in biotechnological fields such as arrays, microfluidics, cell transfer and encapsulation, lab-on-chip devices, etc.

Following is a table comprising process-wise applications of the four different coating strategies with relevant citations and a brief discussion thereafter (Table 4).

7.1 Application of hydrosilylation strategy

The four hydrophobic coating strategies mentioned in this paper finds extensive use in real-world applications. For example, silicon nanocrystals are HF etched followed by hydrosilylation to get alkyl monolayer passivation as shown in Fig. 7. These nanocrystals are then polymer encapsulated for in vivo diagnostic imaging [99]. Nanopatterning through hydrosilylation is also a very common approach of making MEMS devices [100]. With polysilicon as structural material, oxide film as sacrificial layer and isolation layer typically being silicon nitride, it is possible to prepare surface micromachined sensors or actuators together with integrated electronics on the same substrate [101]. Application of this technology include digital mirrors display [102, 103], air bag deployment [104, 105] and chemical sensor development [106]. Researchers have also shown that the poor hydrolytic stability of silane interphase can be greatly improved by hydrosilylation in

Table 4 Process-wise applications of four different coating strategies

Applications of coating strategies			
Hydrosilylation	Silanization and Sol–gel method	Plasma treatment	DC sputtering
Encapsulated contrast agent for diagnostic imaging [99]	Glassware treatment [111–114]	Gas barrier coating [21, 134, 136–138]	Anti-contamination coating for outdoor insulation [62, 63]
MEMS technology [100–106]	Restorative dentistry [115–120]	High-voltage power transmission [134]	
Fiber-reinforced composite [107, 108]	Surface primer [120]	Optics and microelectronics [135, 139–141]	
Cosmetics, adhesives, lubricants [108], rubber manufacturing [109]	Immunobiosensor development [121, 122]	Cell attachment in biomaterials [136, 139, 140]	
Complex catalyst [108–110]	Scratch resistance coating [67, 123, 124]	Self-cleaning windows [142], low-stiction coating in MEMS devices [136, 141, 143, 144]	
	Anti-reflective coating [66, 68, 84, 88, 97, 98, 124–126]	Scratch resistance coating [137, 141]	
	Dye-sensitized solar cells [127–133]		

fiber-reinforced composites (FRC) made of a blend of triethyleneglycol dimethacrylate (TEGMA) and bisphenol A glycidylmethacrylate (Bis-GMA) monomers and glass or alumina oxide fibers [107], which finds use in orthodontics. The general principle is glass fibers used for strengthening plastics are treated with organic hydrosilylating agent to make it more compatible with polymer (as lower surface tension enhances wetting by polymers) [108]. Fillers in rubbers may be pre-treated similarly by organosilyl trialkoxides to obtain better binding between the filler and rubber [109]. Other applications include paper release coating, cosmetics, pressure sensitive adhesives and lubricants [108]. Hydrosilylation has been called the most important application of platinum in homogenous catalysis. A novel glass fiber-supported Pt complex catalyst for hydrosilylation of styrene and triethylsilane has been reported [110]. Similar reports of complex catalysis by hydrosilylation are abundant in literature [108, 109].

7.2 Application of silanization and sol–gel strategy

Silanization and sol–gel method are mechanistically similar. Glassware is silanized to prevent adsorption of solute to glass surfaces or to increase its hydrophobicity. This is particularly important for low concentration of sticky solutes such as single-stranded nucleic acids and proteins [111]. Hydrophobicity of Pyrex glass after treatment with different chloro and amino silanes under various conditions were evaluated [112, 113]. Aminosilanes were found to be more reactive than chlorosilanes, and optimal conditions were achieved with dimethylamino trimethyl silane applied to acid-treated and dried glasses at 250 °C for 5 min. Application of same conditions to other types of glassware may result in different hydrophobicities and surface resistivities [113, 114]. Silanization finds immense application potential in restorative dentistry. In dental technology, silane coupling agents are used to promote adhesion between luting resin composite cement and a silica-coated base metal or noble metal alloy [115]. There is a plethora of dental silane compounds and they differ in formulations and properties. Usually 1–2 vol % of their pre-hydrolyzed form in 90–95 % ethanol–water solvent is used. Silanes need to be activated by hydrolysis before application. Some researchers have found that a combination of silane plus adhesive enhances post-retention to dentin in the middle and coronal root regions [116]. Researchers also found that application of hydrogen peroxide before silanization increased the bond strength between resin cements and fiber posts [117]. Dental resin composites sometimes contain nanosilica particles or porous diatomites as fillers to reinforce the composite [118, 119]. Although a decrease in particle size leads to more attachment of silanization agent, amount of grafting becomes independent of surface area in an area of 1 nm^2 and there is always a competition with sorbed water on the surface [118].

Dental silanes have alkoxy groups on one end which upon hydrolysis react with ceramic surface and C=C on the other end that polymerize with the monomers of resin matrix. Although 3-methacryloxypropyltrimethoxysilane (MPS) is the most commonly used silanizing agent in dentistry, a combination of different silanizing agents or a combination of silanizing agent and etchant is more beneficial [120]. A high critical surface energy on the substrate surface and low surface tension of a liquid is desired

because liquids will spread evenly onto the surface. This is the principle behind its application as surface primer as well [120]. The method of silanization using 3-aminopropyltriethoxysilane (APTES) has been widely used in biosensor development and lab-on-chip application. Immunoglobulin G (IgG) concentration can be determined, from its resonant frequency shift due to complex formation, using APTES-modified piezoelectric crystals coated with protein G [121]. Smoothness or uniform coverage of aminated films have often time been a concern which can be manipulated by varying reaction conditions [122].

Sol–gel-derived nanoporous silica film is based on the basic principle of silanization strategy. Acid- or base-catalyzed or sometimes a combination of acid- and base-catalyzed processes are effective in producing scratch-resistant [67, 123, 124] and anti-reflective [66, 68, 84, 88, 97, 98, 124–126] coating on glass surface. The increase in strength and abrasion resistance is attributed to cross-linking of silica particles in sol and more siloxane (–Si–O–Si–) bond formation [123] and the anti-reflective property stemming from porosity change and hence change in refractive index [66, 67]. The average transmittance of BK7 glass coated in this way increased to 98.5–99.5 % over the range of 500–850 nm [67, 124]. The pencil hardness of the film also reaches 5H and only a little transmittance decline occurs after 100 times rubbing, displaying remarkable abrasion resistance property [89].

Dye-sensitized solar cells (DSSC) are an economically viable and technically simpler alternative to silicon-based solar cells. Nanocrystalline mesoporous silica (SiO_2) [127] or titanium dioxide (TiO_2) [128–130] or hybrid SiO_2–TiO_2 film [131] can be made by sol–gel method, which can effectively increase the light transmittance and photo-conversion efficiency in DSSC solar cells. Literature shows that polymer electro-spinning [127], soft templating with polymer [129] and hard templating with zinc oxide [129, 131] can optimize the properties further, improving the photovoltaic efficiency by 3, 6.7 and 5.6 %, respectively. Introduction of a sol–gel-derived Nb_2O_5 or TiO_2 blocking layer in between fluorinated tin oxide (FTO) electrode and photoanode helps prevent electron back migration and improves efficiency further [132, 133].

7.3 Application of plasma treatment strategy

Dielectric barrier discharges or DBD can be used to make glass surface hydrophobic through plasma treatment, either nonthermal [21, 134–136] or microwave activated [137]. The surface properties (contact angle, surface energy etc.) can be tuned by plasma dose (product of average discharge power and treatment time) [134, 137]. This technique is used in gas barrier coating [21, 134, 136–138], high voltage power transmission [134], optics and microelectronics [137, 139–141], cell attachment to biomaterials [136, 139, 140], self-cleaning windows [142] and low-stiction coating in MEMS device [136, 141, 143, 144].

Automobile windshields need to be scratch-free and tri alkoxy silane-based hydrophobic approach works very well. Research shows that this can be achieved either by plasma treatment [137, 141] or silanization strategy; however, the durability study of contact angle vs. time in hours reflect plasma treatment to be 5 times more durable [141].

7.4 Application of DC sputtering strategy

One outstanding application of DC sputtering strategy is the anti-contamination coating for outdoor insulators [62, 63]. Porcelain and glass have been used as outdoor insulator for decades, but due to their high surface energy it attracts airborne pollutants from wind, nearby industries, smokes and coasts. These pollutants become conducting due to fog, mist or rainfall and cause leakage current, sparks and ultimately complete breakdown of power system. Researchers have proposed the usage of DC sputtered nanocrystalline hafnium oxide (HfO_2) water-repellent coating on the surface of insulators and have studied its self-cleaning and optical transmittance as a function of DC sputtering power and frequency [62, 63]. This work holds lot of promise.

8 Conclusion

This article reviews the principles and mechanisms of glass surface cleaning by various wet chemical and dry cleaning methods and makes a comparative study out of it. This article also covers four major hydrophobic coating strategies, namely hydrosilylation, silanization, plasma treatment and DC sputtering. A special emphasis is given on the silanization process: its mechanism, factors affecting, choices of solvents and precursors, and limitations, which is mechanistically similar to sol–gel method and is utilized in anti-reflective coating as well. Some of the common surface analytical techniques, its utility and reported data have also been reviewed in this context. Finally, a section has been devoted to anti-reflective (AR) and hence light transmittance properties, elucidating the theory and methods of AR coating generation, factors affecting and related literature reports. The challenge lies in coming up with non-harsh cleaning procedures (methods that do not use aggressive chemicals like piranha, hydrofluoric acid, concentrated sulfuric acid, etc.) and water-based hydrophobic coatings (coatings that use water as solvent), with an eye for eco-friendly applications such as in situ application on greenhouse glasses or excavation of archaeological objects.

Acknowledgments This literature review is the stepping stone for a research project, which is being funded by Enterprise Ireland and Keelings Farm.

References

1. Trier F. The glass surface and ways of its modification. www.ksr.tul.cz/glassman/download/10_05_10-00-Trier.pdf
2. Kern W, Puotinen DA (1970) Cleaning solutions based on hydrogen peroxide for use in silicon semiconductor technology. RCA Rev 31:187–206
3. Shriver-Lake LC (1998) Silane-modified surfaces for biomaterial immobilization. In: Cass T, Ligler FS (eds) Immobilized biomolecules in analysis: a practical approach. Oxford University Press, London, pp 1–14
4. Cras JJ, Rowe-Taitt CA, Nivens DA, Ligler FS (1999) Comparison of chemical cleaning methods of glass in preparation for silanization. Biosens Bioelectron 14:683–688
5. Han Y, Mayer D, Offenhäusser A, Ingebrandt S (2006) Surface activation of thin silicon oxides by wet cleaning and silanization. Thin Solid Films 510:175–180
6. Hattori A (1997) Measurement of glass surface contamination. J Non-Cryst Solids 218:196–204
7. Iglauer S, Salamah A, Sarmadivaleh M, Liu K, Phan C (2014) Contamination of silica surfaces: impact on water–CO_2–quartz and glass contact angle measurements. Int J Greenh Gas Control 22:325–328
8. Kondoh E, Baklanov MR, Jonckx F, Maex K (1998) Characterisation of HF-last cleaning of ion-implanted Si Surfaces. Mater Sci Semicond Process 1:107–117
9. Anguita J, Briones F (1998) HF/H_20 vapor etching of SiO_2 sacrificial layer for large-area surface-micromachined membranes. Sens Actuators A 64:247–251
10. Legtenberg R, Tihnans HAC, Elders J, Elwenspoek M (1994) Stiction of surface micromachined structures after rinsing and drying: model and investigation of adhesion mechanisms. Sens Actuators A 43:230–238
11. Lee JH, Jang WI, Lee CS, Lee Y, Choi CA, Baek JT, Yoo HJ (1998) Characterization of anhydrous HF gas-phase etching with CH_3OH for sacrificial oxide removal. Sens Actuators A 61:27–32
12. Rafols C, Herodes K, Beltran JL, Bosch E, Roses M (1997) Ionic equilibria in aqueous organic solvent mixtures The equilibria of HF in an ethanol + water mixture used for cleaning up semiconductors. J Electroanal Chem 433:77–83
13. Martin AR, Baeyens M, Hub W, Mertens PW, Kolbesen BO (1999) Alkaline cleaning of silicon wafers: additives for the prevention of metal contamination. Microelectron Eng 45:197–208
14. Abd-Allah R (2013) Chemical cleaning of soiled deposits and encrustations on archaeological glass: a diagnostic and practical study. J Cult Herit 14:97–108
15. Pulker H, Pulker HK (1999) Coatings on glass, 2nd edn. Elsevier, Amsterdam, pp 63–64
16. Bolon DA, Kunz CO (1972) Ultraviolet depolymerization of photoresist polymers. J Polym Eng Sci 12:109–111
17. Vig JR, Cook CF Jr, Schwidtal K, LeBus JW, Hafner E (1974) In: Proceedings of 28th annual symposium on frequency control, Philadelphia, PA, AD 011113, pp 96–108
18. Vig JR, LeBus JW, Filler RL (1975) In: Proceedings of 29th annual symposium on frequency control, Philadelphia, PA, AD A017466, pp 220–229
19. Vig JR (1976) IEEE TransParts Hybrids Packag PHP 12(4):365–370
20. Vig JR (1993) Chapter 6, Ultraviolet-ozone cleaning of semiconductor surfaces. In: Kern Werner (ed) Handbook of semiconductor wafer cleaning technology, science technology and applications. Noyes Publications, Park Ridge
21. Wang C, He X (2006) Preparation of hydrophobic coating on glass surface by dielectric barrier discharge using a 16 kHz power supply. Appl Surf Sci 252:8348–8351
22. Xu XJ (2001) Dielectric barrier discharge—properties and applications. Thin Solid Films 390:237–242
23. Pochner K, Neff W, Lebert R (1995) Atmospheric pressure gas discharges for surface treatment. Surf Coat Technol 74(75):394
24. Napartovich AP (2001) Overview of atmospheric pressure discharges producing nonthermal plasma. Plasmas Polym 6:1–14
25. Sakuhana S (1985) Fundamentals and applications for glass surface. Uchida Rokaku-Ho Pub, Tokyo, pp 103–107 **(in Japanese)**
26. Yamamoto T, Okubo M, Imai N, Mori Y (2004) Improvement on hydrophilic and hydrophobic properties of glass surface treated by nonthermal plasma induced by silent corona discharge. Plasma Chem Plasma Process 24:1–12
27. Birch WR (2013) Cleaning glass surfaces. In: Aegerter MA, Mennig M (eds) Sol–Gel Technologies for Glass Producers and Users. Springer, Berlin
28. Lu YF, Aoyagi Y (1994) Laser cleaning—a new surface cleaning method without pollutions. MRS Proc 344:329
29. Elnaggar A, Mohamed H, Mahgoub G, Fouad M (2010) Roman glass: removal of burial encrustation and corrosion products. Stud Conserv 55:80–84
30. Weng T-S, Tsai C-H (2014) Laser-induced backside wet cleaning technique for glass substrates. Appl Phys A 116:597–604
31. White ML (1970) The detection and control of organic contaminants on surfaces. In: Goldfinger G (ed) Clean Surfaces: Their Preparation and Characterization for Interfacial Studies. Marcel Dekker, New York, pp 361–373
32. Flinn DH, Guzonas DA, Yoon R-H (1994) Characterization of silica surfaces hydrophobized by octadecyltrichlorosilane. Colloids Surf A Physiochem Eng Asp 87:163–176
33. Saraji S, Goual L, Piri M, Plancher H (2013) Wettability of supercritical carbondioxide/water/quartz systems: simultaneous measurement of contact angle and interfacial tension at reservoir conditions. Langmuir 29:6856–6866
34. Zisman WA (1964) In: Fowkes FM (ed) Contact angle, wettability and adhesion, advances in chemistry series, vol 43. American Chemical Society, Washington, p 1
35. Somasundaran P (1970) Pretreatment of mineral surfaces and its effect on their properties. In: Goldfinger G (ed) Clean Surfaces: Their Preparation and Characterization for Interfacial Studies. Marcel Dekker, New York, pp 285–306
36. Palik ED, Bermudez VM, Glembocki OJ (1985) Ellipsometric study of orientation-dependent etching of silicon in aqueous KOH. J Electrochem Soc 132:871–884
37. Palik ED, Glembocki OJ, Heard I Jr, Bruno PS, Tenerz L (1991) Etching roughness for (100) silicon surfaces in aqueous KOH. J Appl Phys 70(6):3291–3300
38. Adamson AW, Ling I (1964) The status of contact angle as a thermodynamic property. Adv Chem Ser 43:57–73
39. Donose BC, Taran E, Vakarelski IU, Shinto H, Higashitani K (2006) Effects of cleaning procedures of silica wafers on their friction characteristics. J Colloid Interface Sci 299:233–237
40. Genzer J, Efimenko K (2006) Recent developments in superhydrophobic surfaces and their relevance to marine fouling: a review. Biofouling 22:339–360
41. Palacios JC, Cruz GJ, Olayo MG, Chavez Carvayar JA (2009) Characterization of hydrophobic and hydrophilic polythiophene–silver–copper thin film composites synthesized by DC glow discharges. Surf Coat Technol 203:3032–3036

42. Dey T (2011) Nano-scale height manipulation in Sputter-deposited Photolithographic Patterns. J Optoelectron Adv Mater 13:251–254
43. Buriak JM (1999) Functionalization of silicon surfaces for device applications. J Lab Autom 4:36–39
44. Yu WH, Kang ET, Neoh KG (2003) Electroless metallization of hydrogen-terminated silicon surface functionalized by Viologen. Proc Electrochem Soc 13:137–146
45. http://nsl.caltech.edu/research:surfaces
46. http://www.silicone.jp/e/catalog/pdf/SilaneCouplingAgents_e.pdf
47. Bhatia SK, Teixeira JL, Anderson M, Shriver-Lake LC, Calvert JM, Georger JH, Hickman JJ, Dulcey CS, Schoen PE, Ligler FS (1993) Fabrication of surfaces resistant to protein adsorption and application to two–dimensional protein patterning. Anal Biochem 208:197–205
48. Kurth DG, Bein T (1993) Surface reactions on thin layers of silane coupling agents. Langmuir 9:2965–2973
49. Hong H-G, Jiang M, Sligar SG, Bohn PW (1994) Cysteine-specific surface tethering of genetically engineered cytochromes for fabrication of metalloprotein nanostructures. Langmuir 10:153–158
50. Ambrohewicz D, Ciesielczyk F, Nowacka M, Karasiewicz J, Piasecki A, Maciejewski H, Jesionowski T (2013) Fluoroalkylsilane versus alkylsilane as hydrophobic agents for silica and silicates. J Nanomater. Article ID 631938. doi:10.1155/2013/631938
51. Smith EA, Chen W (2008) How to prevent the loss of surface functionality derived from aminosilanes. Langmuir 24(21): 12405–12409
52. Fiorilli S, Rivolo P, Descrovi E, Ricciardi C, Pasquardini L, Lunelli L, Vanzetti L, Pederzolli C, Onida B, Garrone E (2008) Vapor-phase self-assembled monolayers of aminosilane on plasma-activated silicon substrates. J Colloid Interface Sci 321:235–241
53. Metwalli E, Haines D, Becker O, Conzone S, Pantano CG (2006) Surface characterizations of mono-, di-, and tri-aminosilane treated glass substrates. J Colloid Interface Sci 298:825–831
54. Arkles B (2006) Hydrophobicity, hydrophilicity and silanes. Paint Coat Ind Mag. Oct 2006
55. Vansant EF, Van Der Voort P, Vrancken KC (1995) Characterization and chemical modification of the silica surface. Elsevier, Amsterdam
56. Hozumi A, Yokogawa Y, Kameyama T, Sugimura H, Hayashi K, Shirayama H, Takai O (2001) Amino-terminated self-assembled monolayer on a SiO_2 surface formed by chemical vapor deposition. J Vac Sci Technol A 19:1812–1816
57. Siqueira Petri DF, Wenz G, Schunk P, Schimmel T (1999) An improved method for the assembly of amino-terminated monolayers on SiO_2 and the vapor deposition of gold layers. Langmuir 15:4520–4523
58. Wasserman SR, Tao Y-T, Whitesides GM (1989) Structure and reactivity of alkylsiloxane monolayers formed by reaction of alkyltrichlorosilanes on silicon substrates. Langmuir 5:1074–1087
59. Dey T (2011) Colloidal crystalline array of hydrogel-coated silica nanoparticles: effect of temperature and core size on photonic properties. J Sol–Gel Sci Technol 57:132–141
60. Krasnoslobodtsev AV, Smirnov SN (2002) Effect of water on silanization of silica by trimethoxysilanes. Langmuir 18:3181–3184
61. McGovern ME, Kallury KMR, Thompson M (1994) Role of solvent on the silanization of glass with octadecyltrichlorosilane. Langmuir 10:3607–3614
62. Dave V, Dubey P, Gupta HO, Chandra R (2013) Influence of sputtering pressure on the structural, optical and hydrophobic properties of sputtered deposited HfO_2 coatings. Thin Solid Films 549:2–7
63. Dave V, Gupta HO, Chandra R (2014) Influence of sputtering pressure on the structural, optical and hydrophobic properties of sputtered deposited HfO_2 coatings. Appl Surf Sci 295:231–239
64. Pereira L, Barquinha P, Fortunato E, Martins R (2005) Influence of the oxygen/argon ratio on the properties of sputtered hafnium oxide. Mater Sci Eng, B 118:210–213
65. Owens DK, Wendt RC (1969) Estimation of the surface free energy of polymers. J Appl Polym Sci 13:1741–1747
66. Xiao Y, Shen J, Xie Z, Zhou B, Wu G (2007) Microstructure control of nanoporous silica thin film prepared by sol–gel process. J Mater Sci Technol 23:504–508
67. Meng X, Wang Y, Wang H, Zhong J, Chen R (2013) Preparation of the multifunctional antireflective films from a templating composite silica sol with entwining structures. Surf Coat Technol 236:518–524
68. Mahadik SA, Kavale MS, Mukherjee SK, Rao AV (2010) Transparent superhydrophobic silica coatings on glass by sol–gel method. Appl Surf Sci 257:333–339
69. Aptekar JW, Cassidy MC, Johnson AC, Barton RA, Lee M, Ogier AC, Vo C, Anahtar MN, Ren Y, Bhatia SN, Ramanathan C, Cory DG, Hill AL, Mair RW, Rosen MS, Walsworth RL, Marcus CM (2009) Silicon nanoparticles as hyperpolarized magnetic resonance imaging agents. ACS Nano 3(12):4003–4008
70. Carre A, Lacarriere V (2006) Study of surface charge properties of minerals and surface-modified substrates by wettability measurement. In: Mittal KL (ed) Contact Angle, Wettability and Adhesion, vol 4. VSP/Brill, Leiden, pp 1–14
71. Johansson U, Holmgren A, Forsling W, Frost RL (1999) Adsorption of silane coupling agents onto kaolinite surfaces. Clay Miner 34:239–246
72. Young T (1805) An essay on the cohesion of fluids. Philos Trans R Soc Lond 95:65–87
73. Wenzel RN (1936) Resistance of solid surfaces to wetting by water. Ind Eng Chem 28:988–994
74. Khranovskyy V, Ekblad T, Yakimova R, Hultman L (2012) Surface morphology effects on the light-controlled wettability of ZnO nanostructures. Appl Surf Sci 258:8146–8152
75. Henry F, Renaux F, Coppee S, Lazzaroni R, Vandencasteele N, Reniers F, Snyders R (2012) Synthesis of superhydrophobic PTFE-like thin films by self-nanostructuration in a hybrid plasma process. Surf Sci 606:1825–1829
76. Saarikoski I, Korpela FJ, Suvanto M, Pakkanen TT (2012) Superhydrophobic elastomer surfaces with nanostructured micronails. Surf Sci 606:91–98
77. Wu K-R, Wang J-J, Liu W-C, Chen Z-S, Wu J-K (2006) Deposition of graded TiO_2 films featured both hydrophobic and photo-induced hydrophilic properties. Appl Surf Sci 252: 5829–5838
78. Messner R (1947) Importance of interference in increasing metallic reflection, and its practical utilization in optics. Optik 2:228–334
79. Vong MSW, Sermon PA (1997) Observing the breathing of silica sol–gel-derived anti-reflection optical coatings. Thin Solid Films 293:185–195
80. Chapter 4: Antireflection coatings made by a sol–gel process. University of Groningen, thesis
81. Gombert A, Glaubitt W, Rose K, Dreibholz J, Bläsi B, Heinzel A, Sporn D, Döll W, Wittwer V (1999) Subwavelength-structured antireflective surfaces on glass. Thin Solid Films 351:73–78
82. Chen D (2001) Anti-reflection (AR) coatings made by sol–gel processes: a review. Sol Energy Mater Sol Cells 68:313–336
83. Yoldas BE, Partlow PW (1985) Formation of broad band antireflective coatings on fused silica for high power laser applications. Thin Solid Films 129:1–14
84. Beganskiene A, Sakirzanovas S, Kazadojev I, Melninkaitis A, Sirutkaitis V, Kareiva A (2007) Sol–gel derived antireflective

coating with controlled thickness and reflective index. Mater Sci-Pol 25(3):817–824
85. Suratwala TI, Hanna ML, Miller EL, Whitman PK, Thomas IM, Ehrmann PR, Maxwell RS, Burnham AK (2003) Surface chemistry and trimethylsilyl functionalization of Stöber silica sols. J Non-Cryst Solids 316:349–363
86. Stöber W, Fink A, Bohn E (1968) Controlled growth of monodisperse silica spheres in the micron size range. J Colloid Interface Sci 26:62–69
87. San Vicente G, Bayón R, Germán N, Morales A (2009) Long-term durability of sol–gel porous coatings for solar glass covers. Thin Solid Films 517:3157–3160
88. Liu B-T, Yeh W-D (2010) Antireflective surface fabricated from colloidal silica nanoparticles. Colloids Surfaces A Physicochem Eng Aspects 356:145–149
89. Meng X, Wang Y, Wang H, Zhong J, Chen R (2014) Preparation of hydrophobic and abrasion-resistant silica antireflective coatings by using a cationic surfactant to regulate surface morphologies. Sol Energy 101:283–290
90. Husing N, Schubert U (1998) Aerogels—airy materials: chemistry, structure, and properties. Angew Chem Int Ed 37:22–45
91. Pakonk GM, Elaloui E, Achard P, Chevalier B, Chevalier JL, Durant M (1995) Physical properties of silica gels and aerogels prepared with new polymeric precursors. J Non-Crys Sol 186:1–8
92. Ehrburger-Dolle F, Dallamano J, Elaloui E, Pajonk G (1995) Relations between the texture of silica aerogels and their preparation. J Non-Crys Sol 186:9–17
93. Borne A, Chevalier B, Chevalier JL, Quenard D, Elaloui E, Lambard J (1995) Characterization of silica aerogel with the atomic-force microscope and SAXS. J Non-Crys Sol 188:235–242
94. Wu G, Wang J, Shen J, Yang T, Zhang Q, Zhang F (2000) A novel route to control refractive index of sol–gel derived nano-porous silica films used as broadband antireflective coatings. Mater Sci Eng B 78:135–139
95. Wang B, Wilkes Hendrick JC, Liptak SC, McGrath JE (1991) New high-refractive-index organic/inorganic hybrid materials from sol–gel processing. Macromolecules 24:3449–3450
96. Haereid S, Dahle M, Lima S, Einarsrud M (1995) Preparation and properties of monolithic silica xerogels from TEOS-based alcogels aged in silane solutions. J Non-Crys Sol 186:96–103
97. Prado R, Beobide G, Marcaide A, Goikoetxea J, Aranzabe A (2010) Development of multifunctional sol–gel coatings: anti-reflection coatings with enhanced self-cleaning capacity. Sol Energy Mater Sol Cells 94:1081–1088
98. Rutan M (2011) Abrasion resistant anti-reflective sol–gel coatings. High School Reports, University of Rochester http://www.lle.rochester.edu/media/publications/high_school_reports/documents/hs_reports/2011/Rutan.pdf
99. Hessel CM, Rasch MR, Hueso JL, Goodfellow BW, Akhavan VA, Puvanakrishnan P, Tunnell JW, Korgel BA (2010) Alkyl passivation and amphiphilic polymer coating of silicon nanocrystals for diagnostic imaging. Small 6:2026–2034
100. Maboudian R (1998) Surface processes in MEMS technology. Surf Sci Rep 30:207–269
101. Howe RT, Boser BE, Pisano AP (1996) Polysilicon integrated microsystems: technologies and applications. Sens Actuators, A 56:167–177
102. Hornbeck LJ (1993) In: Proceedings of IEEE international electron devices meeting, Washington, DC, pp 381–384
103. Sampsell JB (1994) Digital micromirror device and its application to projection displays. J Vac Sci Technol B 12: 3242–3246
104. Payne RS, Sherman S, Lewis S, Howe RT (1995) In: Proc. IEEE Int. Solid-State Circuits Conf, San Francisco, CA, pp 164–165
105. Chau KH-L et al (1995) In: Proceedings of 8th international conference on solid-state sensors and actuators—Transducers'95, Stockholm, Sweden, pp 593–596
106. Trimmer WS (1996) Micromechanics and MEMS, Classic and Seminal Papers to 1990. IEEE Press, New York
107. Jancar J, Polacek P (2011) Hydrolytically stable interphase on alumina and glass fibers via hydrosilylation. Compos Interfaces 18:633–644
108. Van Leeuwen PWNM (2004) Homogenous catalysis: understanding the art. Kluwer, Dordrecht, pp 372–373
109. Marciniec B (2009) Functionalisation and cross-linking of organosilicon polymers, In: Marciniec B (ed) Hydrosilylation: a comprehensive review on recent advances, Springer, Netherlands, pp 159–189 (chapter 5)
110. Yang HT, Fang ZP, Fu XY, Tong LF (2008) Preparation of glass fiber-supported platinum complex catalyst for hydrosilylation reactions. Catal Commun 9:1092–1095
111. Seed B (2001) Appendix: 3K silanizing glassware. Curr protoc Immunol 21:3KA 1-2
112. Deyhimi F, Coles JA (1982) Rapid silylation of a glass surface: choice of reagent and effect of experimental parameters on hydrophobicity. Helv Chim Acta 65:1752–1759
113. Ammann D (1986) Ion-selective microelectrodes: principles design and application. Springer, Berlin
114. Munoz J-L, Deyhimi F, Coles JA (1983) Silanization of glass in the making of ion-selective microelectrodes. J Neurosci Methods 8:231–247
115. Ying C, Lung K, Matinlinna JP (2014) Surface pretreatment methods and silanization. In: Matinlinna JP (ed) Handbook of oral biomaterials. Pan Stanford Publishing, Singapore
116. Machado FW, Bossardi M, Ramos TS, Valente LL, Munchow EA, Piva E (2015) Application of resin adhesive on the surface of a silanized glass fiber-reinforced post and its effect on the retention to root dentin. J Endod 41:106–110
117. Mosharraf R, Ranjbarian P (2013) Effects of post surface conditioning before silanization on bond strength between fiber post and resin cement. J Adv Prosthodont 5:126–132
118. Karabela MM, Sideridou I (2011) Synthesis and study of properties of dental resin composites with different nanosilica particles size. Dent Mater 27:825–835
119. Miao X, Zhu M, Li Y, Zhang Q, Wang H (2012) Synthesis of dental resins using diatomite and nano-sized SiO_2 and TiO_2. Prog Nat Sci Mater Int 22:94–99
120. Ho GW, Matinlinna JP (2011) Insights on ceramics as dental materials. Part II: Chem Surface Treat 3:117–123
121. Suri CR, Mishra GC (1996) Activating piezoelectric crystal surface by silanization for microgravimetric immunobiosensor application. Biosens Bioelectron 11:1199–1205
122. Howarter JA, Youngblood JP (2006) Optimization of silica silanization by 3-aminopropyltriethoxysilane. Langmuir 22: 11142–11147
123. Wang J, Wu G, Shen J, Yang T, Zhang Q, Zhou B, Deng Z, Fan B, Zhou D, Zhang F (2000) Scratch-resistant improvement of sol–gel derived nano-porous silica films. J Sol–Gel Sci Technol 18:219–224
124. Li X, Shen J (2011) A scratch-resistant and hydrophobic broadband antireflective coating by sol–gel method. Thin Solid Films 519:6236–6240
125. Puetz J, Gasparro G, Aegerter MA (2003) Liquid film spray deposition of transparent conducting oxide coatings. Thin Solid Films 442:40–43
126. Mahadik SA, Mahadik DB, Kavale MS, Parale VG, Wagh PB, Barshilia HC, Gupta SC, Hegde PND, Rao AV (2012) Thermally stable and transparent superhydrophobic sol–gel coatings by spray method. J Sol–Gel Sci Technol 63:580–586

127. Raut HK, Nair AS, Dinachali SS, Ganesh VA, Walsh TM, Ramakrishna S (2013) Porous SiO_2 anti-reflective coatings on large-area substrates by electrospinning and their application to solar modules. Sol Energy Mater Sol Cells 111:9–15
128. Muniz EC, Goes MS, Silva JJ, Varela JA, Joanni E, Parra R, Bueno PR (2011) Synthesis and characterization of mesoporous TiO_2 nanostructured films prepared by a modified sol–gel method for application in dye solar cells. Ceram Int 37:1017–1024
129. Yun TK, Park SS, Kim D, Hwang Y-K, Huh S, Bae JY, Won YS (2011) Pore-size effect on photovoltaic performance of dye-sensitized solar cells composed of mesoporous anatase-titania. J Power Sources 196:3678–3682
130. Dhungel SK, Park JG (2010) Optimization of paste formulation for TiO_2 nanoparticles with wide range of size distribution for its application in dye sensitized solar cells. Renewable Energy 35:2776–2780
131. Ye L, Zhang Y, Zhang X, Hu T, Ji R, Ding B, Jiang B (2013) Sol–gel preparation of $SiO_2/TiO_2/SiO_2$–TiO_2 broadband antireflective coating for solar cell cover glass. Sol Energy Mater Sol Cells 111:160–164
132. Kim J, Kim J (2011) Fabrication of dye-sensitized solar cells using Nb_2O_5 blocking layer made by sol–gel method. J Nanosci Nanotechnol 11:7335–7338
133. Lee JG, Cheon JH, Yang HS, Lee DK, Kim JH (2012) Enhancement of photovoltaic performance in dye-sensitized solar cells with the spin-coated TiO_2 blocking layer. J Nanosci Nanotechnol 12:6026–6030
134. Fang Z, Qiu Y, Kuffel E (2004) Formation of hydrophobic coating on glass surface using atmospheric pressure non-thermal plasma in ambient air. J Phys D Appl Phys 37:2261–2266
135. Krumpolec R, Zahoranova A, Cernak M, Kovacik D (2012) Deposition of hydrophobic polymer films by atmospheric pressure plasma polymerization. In: WDS'12 Proceedings of contributed papers, part III, pp 24–29
136. Barankin MD, Gonzalez E II, Habib SB, Gao L, Guschl PC, Hicks RF (2009) Hydrophobic films by atmospheric plasma curing of spun-on liquid precursors. Langmuir 25:2495–2500
137. Ting JAS, Rosario LMD, Lee HV Jr, Ramos HJ, Tumlos RB (2014) Hydrophobic coating on glass surfaces via application of silicone oil and activated using a microwave atmospheric plasma jet. Surf Coat Technol 259:7–11
138. Teshima K, Sugimura H, Inoue Y, Takai O (2003) Gas barrier performance of surface-modified silica films with grafted organosilane molecules. Langmuir 19:8331–8334
139. Tsuji H, Sommani P, Hayashi Y, Kojima H, Sato H, Gotoh Y, Takaoka G, Ishikawa J (2011) Surface modification of silica glass by CHF_3 plasma treatment and carbon negative-ion implantation for cell pattern adhesion. Surf Coat Technol 206:900–904
140. Philipavičius J, Kazadojev I, Behanskienė A, Melninkaitis A, Sirutkaitis V, Kareiva A (2008) Mater Sci 14(4):283–287
141. Yamamoto T, Okubo M (2007) Nonthermal Plasma Technology. In: Wang LK, Hung Y-T, Shammas NK (eds) Advanced physicochemical treatment technologies. Handbook of environmental engineering, vol. 5. Springer, Humana Press, Totowa
142. Balu B, Breedveld V, Hess DW (2008) Fabrication of "roll-off" and "sticky" superhydrophobic cellulose surfaces via plasma processing. Langmuir 24:4785–4790
143. Hayashi K, Saito N, Sugimura H, Takai O, Nakagiri N (2002) Regulation of the surface potential of silicon substrates in micrometer scale with organosilane self-assembled monolayers. Langmuir 18:7469–7472
144. Jung G-Y, Li Z, Wu W, Chen Y, Olynick DL, Wang S-Y, Tong WM, Williams RS (2005) Vapor-phase self-assembled monolayer for improved mold release in nanoimprint lithography. Langmuir 21:1158–1161